Title: Antigen presentation by class I molecules on brain endothelium dynamically regulates T-cell mediated neuropathology in experimental cerebral malaria

[1,5]Fain, CE, [3,5]Zheng, J, [1]Jin, F, [1]Ayasoufi, K, Wu, Y, [5]Lilley, MT, [1,5]Dropik, AR, [1]Wolf, DM, Rodriguez, RC, [4,5]Aibaidula, A, [1,5]Tritz, ZP, [5]Bouchal, SM, [7]Pewe, LL, [7]Urban, SL, [1,5]Chen, [6]Y, Chang, S, [1]Hansen, MJ, [9]Kachergus, JM, [9]Shi, J, [9]Thompson, EA, [7]Harty, JT, [6]Parney, IF, [8]Sun, J, [1,3]Wu, LJ, [1,2,3]Johnson, AJ*

[1] Mayo Clinic Department of Immunology, Rochester, MN
[2] Mayo Clinic Department of Molecular Medicine, Rochester, MN
[3] Mayo Clinic Department of Neurology, Rochester, MN
[4] Mayo Clinic Department of Molecular Pharmacology and Experimental Therapeutics
[5] Mayo Clinic Graduate School of Biomedical Sciences, Rochester, MN
[6]Mayo Clinic Department of Neurosurgery, Rochester, MN
[7]University of Iowa Department of Pathology, Iowa City, IA
[8]University of Virginia Department of Medicine, Charlottesville, VA
[9]Mayo Clinic Department of Cancer Biology, Jacksonville, FL

Authors have no conflicts or competing interests to disclose.

Author contributions: CEF, JZ, FJ, KA, MTL, ARD, DMW, RCR, AA, and ZPT assisted with experiments. CEF, JZ, FJ, YW, SMB, YC, JMK, and JS analyzed data. CEF and AJJ designed experiments and interpreted results. CEF wrote the manuscript. All authors provided feedback for editing, read manuscript, and agree with data presented.

*Correspondence to Aaron J. Johnson, PhD
Professor and Consultant
Departments of Immunology, Neurology, and Molecular Medicine
Guggenheim 4-11C
Mayo Clinic
200 First St. SW
Rochester, MN 55905
Johnson.aaron2@mayo.edu
Tel: (507) 266-1973

Abstract

CD8 T cells are implicated in the neuropathology of human cerebral malaria. Using human data as well as the *Plasmodium berghei* ANKA (PbA) model of experimental cerebral malaria (ECM), we sought to define contributions of brain endothelial cell MHC class I antigen (Ag) presentation to CD8 T cells in this pathology. We crossed novel H-2K^b and H-2D^b LoxP mice to Cdh5-Cre mice to achieve targeted deletion of discrete class I molecules on endothelium. RNA transcriptomes of brains during PbA infection are differential between H-2K^b and H-2D^b expressing mice, highlighting differential regulation of neuropathogenesis. Distinct patterns of disease onset, CD8 T cell infiltration, targeted cell death, and regional BBB disruption and vascular leakage are observed. Strikingly, ablation of H-2K^b or H-2D^b from brain endothelial cells resulted in diminished interactions of T cells with brain vasculature and lessened infiltration of activated CD8 T cells, resulting in prevention of blood-brain barrier (BBB) disruption, CNS vascular leakage and death. Overall, endothelium-specific conditional knockout (cKO) mice were protected from development of ECM resulting in survival of the mice. These data show the first *in vivo* evidence that interactions of CD8 T cells and cognate peptide:MHC on brain endothelium regulate development of ECM neuropathology. Therefore, targeting MHC class I interactions therapeutically may hold potential for treatment of cases of severe malaria.

Introduction

Plasmodium falciparum has been classified as the deadliest parasite by the World Health Organization (WHO). This strain is also the most prevalent malaria parasite, accounting for majority of human infections[1]. Despite initiatives to limit mortality, it is estimated that greater than 600,000 people succumbed to malaria in 2020[2]. A severe complication *of Plasmodium falciparum* is severe encephalopathy, termed cerebral malaria (CM), which results in high

62 mortality despite treatment[3, 4, 5, 6, 7]. CM accounts for approximately 80% of all malaria-related
63 deaths, and patient admissions with CM are steadily increasing annually[2]. The majority of
64 cerebral malaria patients are diagnosed by the presence of asexual parasite in a blood smear,
65 deep coma, and absence of other infectious disease[3, 8]. Other hallmarks of disease can only be
66 assessed post-mortem such as disruption of BBB tight junction proteins, vascular permeability,
67 sequestration of parasitized red blood cell (prbc) and leukocytes, cerebral microhemorrhage and
68 endothelial cell activation[9, 10]. MRI has been gaining traction as a diagnostic tool in patients, as
69 vascular permeability can be assessed via T1 and T2 weighted MRI[10]. Recently,
70 immunohistochemical studies of autopsied human brain specimens have revealed that CD8 T
71 cells have been shown to be tightly associated with brain microvasculature and infiltrate brain
72 parenchyma, implying an important role for this immune cell type in neuropathogenesis[11].
73 *Plasmodium berghei ANKA* (PbA) infection is an established murine model that
74 recapitulates human disease and CNS pathology, referred to as ECM[12]. As in the human disease,
75 CD8 T cell responses are strongly implicated in the neuropathology. Importantly, CD8 T cells
76 are required to have functioning cytotoxic capacity to develop the fatal BBB disruption
77 associated with ECM[13, 14, 15, 16]. An IFN-γ dependent upregulation of adhesion molecules (ICAM-
78 1 and VCAM-1) and molecules associated with Ag-presentation (MHC Class I molecules D^b and
79 K^b and MHC Class II) has been observed on brain and meningeal endothelial cells day 6 of PbA
80 infection[17]. However, the contribution of specific cell types producing IFN-γ in this pathology
81 have not been interrogated[17]. Interest in these CD8 T cell-endothelial cell interactions, has
82 prompted a concerted effort to define the requirement of Ag-specific CD8 T cells in this
83 neuropathology. Due to the complex life-cycle of the parasite, defined by extensive antigenic
84 variation throughout each stage, this has proven a difficult task. The engagement of CD8 T cells

85 with class I molecules has been functionally assessed with bone marrow chimeras of MHC class
86 I-deficient hosts reconstituted with class I-sufficient hematopoietic presentation[17]. However, it is
87 known that CD8 T cells raised in these hosts have inherently impaired development and
88 survival[17, 18]. While this important work narrows in on the significance of non-hematopoietic Ag-
89 presentation in this pathology, the role of Ag-presentation specifically on brain vasculature has
90 not yet been addressed. Furthermore, the contribution of discrete class I molecules in ECM
91 pathology remain undefined.

92 In these studies, we sought to define the contribution of mouse brain microvascular
93 endothelial cell (MBMEC) Ag-presentation by discrete class I molecules to the pathogenesis and
94 lethality of ECM. We hypothesized that conditional ablation of Ag-presentation by H-2K^b and
95 H-2D^b class I molecules on MBMECs would result in controlled modulation of activation and
96 entry of parasite-specific CD8 T cells, attenuating pathology. To test this, we crossed
97 endothelium-specific Cdh5-Cre mice with our novel H-2K^b LoxP and H-2D^b LoxP mice to
98 create cKOs of discrete class I molecules. In these studies, we employed human and mouse
99 transcriptomic data to evaluate gene expression in brains in response to plasmodium expression.
100 We also employed *in vivo* 2-photon imaging to interrogate T cell interactions at the inflamed
101 vasculature of the brain when individual MHC class I molecules are present or conditionally
102 deleted on endothelium during PbA infection. Infiltration, activation, and localization of CD8 T
103 cells and their potential targets were assessed via spectral flow cytometry in these novel
104 transgenic mice. We demonstrate that interactions with specific class I molecules determined
105 CD8 T cell activation, infiltration of the brain and localization and onset of cell death and
106 neuropathology. However, knockout of H-2K^b and H-2D^b in endothelial cells prevented CD8 T
107 cell interactions at brain vasculature, CD8 T cell activation, BBB disruption, cell death and

108 neuropathology. These mice did not develop ECM, resulting in almost complete survival.
109 Together these data demonstrate that CD8 T cells engage H-2K^b or H-2D^b class I molecules on
110 MBMECs in order to coordinate activation, entry, and induction of neuropathology. These
111 studies indicate that modulation of brain microvascular endothelial cell class I restricted Ag-
112 presentation may hold therapeutic benefit in cases of cerebral malaria.
113
114 **Results**
115 **Mouse and human brain microvascular endothelial cells increase antigen presentation**
116 **molecules capable of eliciting T cell responses after *Plasmodium* infection.** C57BL/6 mice
117 were intraperitoneally (I.P.) injected with PbA prbcs, resulting in peripheral infection and
118 manifestation of ECM on days 6-8 (Fig. 1a). Brains were harvested and RNA was extracted from
119 whole brains of infected C57BL/6 mice and uninfected controls (Fig. 1a). Nanostring analysis
120 was performed on bulk RNA for analysis of differential gene expression between uninfected and
121 infected mice (Fig. 1b). Upregulated genes were associated with major immunological pathways,
122 including Ag-presentation, T cell responses, cytotoxicity, cell activation and apoptosis.
123 Downregulated genes were associated with markers of homeostasis or components of blood-
124 brain barrier (Fig. 1b). Gene expression data were analyzed using Ingenuity Pathway Analysis
125 (IPA). Causal network analysis identified MHC Class I family as the most significant master
126 regulator in ECM pathology (Supplementary Table 1). MHC Class I family activation led to
127 downstream activation of the majority of upregulated genes of interest identified in Fig. 1b (Fig.
128 1c). Canonical pathway analysis identified the most differentially enriched signaling pathways
129 during ECM, confirming Ag-presentation as a major pathway of interest (Fig. 1d). MBMECs
130 have been implicated to be involved in Ag-presentation during ECM (Fig. 1e). To interrogate

131 their role, we employed enzymatic digestion and high-dimensional spectral flow cytometry to
132 measure expression of Ag-presentation-associated molecules. MHC Class I median fluorescence
133 intensity is increased on MBMECs during ECM and the percent of expression on MBMECs is
134 significantly higher during ECM (Fig. 1f). MHC Class II is a well-known marker of antigen
135 presenting cells (APCs). MHC Class II expression on MBMECs greatly increased from minimal
136 to high during ECM, implicating their role in Ag-presentation (Fig. 1g). We next interrogated
137 gene expression signatures of human brain microvascular endothelial cells (HBMECs) from
138 human donor after exposure to *Plasmodium falciparum*. To this end, we utilized human
139 microarray dataset from Tripathi et al. (accession GSE9861)[19] in NCBI GEO database. In brief,
140 isolated HBMECs were co-cultured with *Plasmodium falciparum* prbcs or uninfected red blood
141 cells in culture and then analyzed (Fig. 1h). We first assessed the distribution of expression
142 values for each human sample to ensure suitability for comparison (Supplementary Fig. 1a).
143 After human sample validation we evaluated MHC Class I and MHC Class II expression levels.
144 MHC Class I expression was significantly increased in HBMECs exposed to *Plasmodium*
145 *falciparum* infected red blood cells (Fig. 1i). Human samples which were exposed to infection
146 were subdivided into two groups 1) high adhesion molecule expression and 2) low adhesion
147 molecule expression[19] (Supplementary Fig. 1b). MHC Class II expression was shown to be
148 significantly upregulated only in the high adhesion molecule samples compared to controls (Fig.
149 1j). Using GEO2R analysis platform, MHC Class I was identified as one of the most
150 significantly differentially expressed genes and was in the top 5 genes with significant
151 upregulation on HBMECs after exposure to *Plasmodium* infection (Supplementary Table 2).
152 When comparing mouse and human genes involved with Ag-presentation we saw that gene
153 activation and inhibition in these pathways were highly analogous (Supplementary Fig. 2). We

154 also saw comparable upregulation of homologous genes of interest downstream of MHC Class I
155 in human HBMECs, consistent with our observations in the mouse model (Fig. 1k). When
156 performing gene set enrichment analysis (GSEA) on HBMEC transcriptomics data we identified
157 the molecular signature for T cell activation involved in immune response to be highly enriched
158 in HBMECs exposed to infection. The enrichment of this gene set indicates that HBMECs
159 become an APC during *Plasmodium* infection, capable of eliciting this downstream T cell
160 response (Fig. 1l). Together, these results suggest that in both mouse and human, brain
161 endothelial cells are performing Ag-presentation to activate downstream T cell effector activities
162 following *Plasmodium* infection.
163
164 **Endothelial cell specific K^b conditional knockout mice develop normal peripheral**
165 ***Plasmodium* infection and immune responses.** We crossed (class I deficient background, K^b-/-,
166 D^b-/-) K^b LoxP mice with (class I deficient background, K^b-/-, D^b-/-) Cdh5-Cre mice (Fig. 2a).
167 The resulting animals are defined as K^b Cre- littermate (with ubiquitous K^b expression), and
168 Cdh5-Cre K^b cKO (with endothelial-specific ablation of K^b), respectively. At baseline, Cdh5-Cre
169 K^b cKO mice had significantly reduced protein levels of K^b on brain endothelium, as well as
170 reduced percentage of brain endothelial cells that express K^b (Fig. 2b-d). T cell development was
171 intact in Cdh5-Cre K^b cKO and K^b Cre- littermates with no changes in thymic T cell subset
172 frequencies, mTEC and cTEC frequencies, or thymic weights between groups (Fig. 2e-f and
173 Supplementary Fig. 3a). Furthermore, no sex specific differences pertaining to T cell
174 development, overt changes in CD8 T cell repertoire, or change in splenic weights were observed
175 (Supplementary Fig. 3b-d). To determine the effect of K^b class I molecule ablation on MBMECs
176 during ECM, adult Cdh5-Cre K^b cKO (~3-month-old) mice and K^b Cre- littermates were I.P.

177 infected with $1x10^6$ PbA prbcs and tissues were harvested at approximately 6-8 days post
178 infection (dpi) (Fig. 2g). During infection K^b remained significantly reduced on brain
179 endothelium (Fig. 2h-j). In the spleen, we observed no changes to granulocyte or APC subsets
180 during infection in Kb Cre- littermates or Cdh5-Cre K^b cKO mice (Fig. 2k-l). Importantly, there
181 were no differences in the ability to establish blood stage infection in these mice (Fig. 2m).
182 Populations of immune cells were assessed in peripheral tissues at baseline and during infection
183 and showed no changes in CD45+ immune cell numbers between Cre- littermates and Cdh5-Cre
184 K^b cKO spleen, peripheral blood or inguinal LN (Supplementary Fig. 3e). In these peripheral
185 tissues CD4 and CD8 T cell numbers and activation state remained unchanged between groups in
186 all peripheral organs, with the exception of a modest reduction in numbers of activated CD8s at
187 baseline in inguinal LNs in the Cdh5-Cre K^b cKO mice (Supplementary Fig. 3g). However,
188 during PbA infection, there were no differences in CD8 activation in inguinal LNs (Fig. 2o).
189 These results demonstrate that our Cdh5-Cre K^b cKO mouse model has efficient deletion of K^b
190 on vasculature, while maintaining a fully functional peripheral immune response to *Plasmodium*
191 infection. This allows us to proceed with interrogation of potentially brain-specific
192 immunomodulatory functions of K^b Ag-presentation by brain endothelial cells in ECM.
193
194 **Endothelial cell specific D^b conditional knockout mice develop normal peripheral**
195 ***Plasmodium* infection and immune responses.**
196 We crossed (class I deficient background, K^b-/-, D^b-/-) D^b LoxP mice with (class I deficient
197 background, K^b-/-, D^b-/-) Cdh5-Cre mice (Fig. 3a). The resulting animals are defined as either D^b
198 Cre- littermate (with ubiquitous D^b expression), or Cdh5-Cre D^b cKO (with endothelial-specific
199 ablation of D^b). Endothelial cell expression of D^b at baseline in Cdh5-Cre D^b cKO mice was

200 comparable to Cre- littermate controls. Percentage of class I expression on endothelium was
201 reduced but did not reach statistical significance in uninfected Cdh5-Cre D^b cKO mice (Fig. 3b-
202 d). T cell development was intact with no changes in thymic T cell subset frequencies, mTEC
203 and cTEC frequencies, or in thymic weights between groups (Fig. 3e-f and Supplementary Fig.
204 4a). There were no differences between males and females in development of thymic T cell
205 subsets, and no differences between groups in CD8 T cell V beta usage in spleen, or in splenic
206 weights (Supplementary Fig. 4b-d). To determine the effect of D^b class I molecule ablation on
207 MBMECs during ECM, adult Cdh5-Cre D^b cKO (~3-month-old) mice were I.P. infected with
208 PbA and tissues were harvested at onset of severe neurological symptoms, approximately 6-8 dpi
209 (Fig. 3g). Importantly, during infection D^b expression was significantly reduced on brain
210 endothelium (Fig. 3h-j). Spleens of these animals had no changes to granulocyte or APC subsets
211 during infection (Fig. 3k-l) and mice established full blood stage infection in the periphery (Fig.
212 3m). Assessment of immune cell populations in peripheral tissues at baseline and during
213 infection revealed no changes in CD45+ immune cell number between D^b Cre- littermates and
214 Cdh5-Cre D^b cKO in spleen, peripheral blood or inguinal LN (Supplementary Fig. 4e-f). CD4
215 and CD8 T cell numbers and activation state remained unchanged between groups in all
216 peripheral organs at baseline (Supplementary Fig. 4f). However, during infection, there was
217 reduction in number of activated CD8 T cells in inguinal LN in the Cdh5-Cre D^b cKO animals
218 (Fig. 3n-p). These results demonstrate that our Cdh5-Cre D^b cKO mouse model has sufficient
219 deletion of D^b on vasculature during PbA infection and a fully functional peripheral immune
220 response. These results enabled us to proceed with interrogation of potentially brain-specific
221 immunomodulatory functions of D^b Ag-presentation by brain endothelial cells in ECM.
222

223 **T cell dynamics at the barrier are modulated by the presence of distinct class I molecules**
224 **on endothelium.** To assess whether brain vasculature was inherently changed by loss of
225 endothelial class I in cKO mice, we performed maximum intensity projections (MIPs) using MRI
226 angiography to illuminate and assess the blood vessels. Cdh5-Cre K^b cKO and Cdh5-Cre D^b
227 cKO were compared to their respective Cre- littermate controls. At baseline, we observed no
228 differences in 3D volume of overall brain vasculature or voxel units (Supplementary Fig. 5a-b
229 and 5c-d). We therefore proceeded to assess the effects of discrete MHC class I molecules on T
230 cell dynamics in brain vasculature. To address this, we employed acute cranial window
231 placement and *in vivo* two-photon imaging after IV injections of anti-Thy1.2-Alexa Fluor 488 to
232 label T cells in vasculature and Texas Red-Dextran to label vessels. 6-7 days following PbA
233 infection, mice underwent live imaging and T cell interactions at the brain vasculature were
234 tracked over time (Fig. 4a). Cre- Littermates with K^b expression on brain vasculature presented
235 with higher numbers of T cells per field of view (FOV) with slowed velocities, indicating
236 interactions with K^b on endothelium (Fig. 4b and 4c). In contrast, Cdh5-Cre K^b cKO mice, which
237 lack K^b on endothelium, had lower numbers of T cells per FOV, with higher velocity indicating
238 less interactions with endothelium (Fig. 4b and 4c). Interestingly, there were no significant
239 differences between the frequency that T cells contacted the vessels between genotypes.
240 However, arrest on vessels was significantly increased when K^b was expressed on the brain
241 vasculature (Fig. 4d-4e and Supplementary Videos 1-2). To investigate these T cell interactions
242 further, we examined the activation state and adhesion molecule expression of MBMECs. During
243 late-stage PbA infection, endothelial cells upregulate adhesion molecules responsible for
244 initiating T cell extravasation[20]. P-selectin, which facilitates activated T cell rolling, did not
245 differ in expression between Cdh5-Cre K^b cKO mice and Cre- littermates (Fig. 4f). ICAM-1 and

246 VCAM-1 expression, involved in arrest and adhesion, also showed no significant differences
247 during infection (Fig. 4g-h). When endothelial cells are activated, they upregulate molecules
248 involved in Ag-presentation[17]. Surprisingly, when K^b class I molecule expression was ablated,
249 MHC Class II molecules were upregulated on brain endothelium during infection (Fig. 4i).
250 T cell dynamics in Cre- D^b expressing and Cdh5-Cre D^b cKO mice were similar to those
251 of the previous model. 6-7 dpi with PbA T cell interactions with vasculature were tracked over
252 time during intravital imaging (Fig. 4j). Cre- Littermates with D^b present on vasculature showed
253 high numbers of T cells/FOV. In Cdh5-Cre D^b cKO mice, T cells were greatly reduced per FOV,
254 indicating fewer T cells slowed down to interact with endothelium when D^b molecule is ablated
255 on vasculature (Fig. 4k). Meanwhile, D^b expressing Cre- littermate T cells had slower velocities,
256 indicating more interactions with D^b on endothelium. When endothelial D^b is conditionally
257 deleted in Cdh5-Cre D^b cKO mice, T cells that interact with vessels had significantly increased
258 velocities, with reduced slowing and rolling on vasculature (Fig. 4l). Again, there were no
259 significant differences between the percentage of T cells contacting vessel walls between groups.
260 However, the frequency of T cell arrests was significantly increased when D^b was expressed by
261 brain vasculature (Fig. 4m and 4n). (Supplementary Videos 2-3). P-selectin was greatly
262 increased when D^b was present on brain endothelium during infection, indicating a higher
263 probability of activated T cell rolling (Fig. 4o). Interestingly, cells/FOV in the D^b expressing Cre-
264 littermates, had increased cells/FOV compared to K^b Cre- littermates (Fig. 4b and 4k). There
265 were no significant changes in ICAM-1 or VCAM-1 expression on endothelium when D^b was
266 conditionally deleted (Fig. 4p-q). As was seen with K^b cKO mice, deletion of D^b class I molecule
267 on endothelial cells resulted in higher expression of MHC Class II molecules on endothelium in
268 comparison to Cre- littermates (Fig.4i and 4r). Together, this data demonstrates that H-2K^b and

269 H-2D^b class I molecules are critical for optimal T cell adhesion and arrest to brain endothelium
270 during ECM.
271
272 **CD8 T cell activation and infiltration into brain parenchyma is differentially modulated by**
273 **discrete class I molecules during infection.** We next addressed if the changes observed in T
274 cell dynamics at the brain vasculature during PbA infection corresponded with T cell infiltration
275 into brain parenchyma. First, we wanted to confirm that cervical lymph node (cLN) priming of
276 brain draining antigens was intact in our mouse models. To test this, we employed Theiler's
277 murine encephalomyelitis virus (TMEV) and TMEV-OVA. These neurotropic viruses are
278 intracranially administered and provide a highly reproduceable model of CNS antigen drainage
279 resulting in cLN priming, CD8 T cell infiltration, and viral clearance[21, 22, 23]. TMEV
280 immunodominant peptide VP2$_{121-130}$ is presented in the H-2D^b MHC class I molecule whereas
281 TMEV-OVA model antigen OVA$_{257-264}$ is presented by H-2K^b [23]. On day 7 post infection mice
282 were perfused and cLNs were analyzed via spectral flow cytometry (Supplementary Fig. 6a). In
283 mice infected with either TMEV or TMEV-OVA, tetramer staining was unchanged between Cre-
284 and Cre+ mice indicating that cLN priming in these mice is intact (Supplementary Fig. 6b-c). We
285 now evaluated immune cell infiltration into the brain in the ECM model, in which the
286 *Plasmodium* infection arises in the periphery prior to neuroinflammation in the brain (Fig. 5a).
287 At moribund, 6-8 d.p.i., mice were euthanized and perfused. Mouse brains were processed into
288 single cell suspensions and analyzed via spectral flow cytometry. Overall immune populations in
289 the brains during infection can be visualized in the UMAP projection (Fig. 5b). Data
290 encompassing CNS infiltration of immune cells were interrogated. Absolute counts of total
291 CD45+ immune cells in the brain remain unchanged when K^b class I molecules are present on

292 endothelium versus endothelial cell class I molecule conditional knockout mice (Supplementary
293 Fig. 6d). Numbers of CD4 T cells in the brain also remain unchanged regardless of K^b expression
294 by endothelial cells (Fig. 5e). However, when K^b expression is lost on endothelium, CD8 T cell
295 infiltration of the brain is greatly diminished (Fig. 5f). Since adhesion molecule expression on
296 endothelium was previously shown to be unchanged, we also examined CD8 T cells for
297 chemokine receptors involved in trafficking to the CNS and adhesion to the endothelium. Levels
298 of CXCR3, a receptor shown to be necessary for recruitment of T cells into the brain to establish
299 ECM[24, 25], was not impacted by ablation of K^b on vasculature (Supplementary Fig. 6f-g). CCR7,
300 a chemokine receptor known to be upregulated on T cells trafficking to the brain during
301 neuroinflammation, was also evaluated[26]. During ECM the olfactory region highly upregulates
302 CCL21, and blockade of CCR7 decreases T cell activation, recruitment and survival[27]. In Cre-
303 littermates with K^b, we saw no difference in CD8 T cell expression of CCR7 from mice lacking
304 K^b on vasculature (Supplementary Fig. 6h-i). We next evaluated effector status of CD4 and CD8
305 T cells in the brain. Interestingly, CD8 T cells that infiltrated the brain during infection produce
306 significantly less IFN-γ when K^b expression was ablated on vasculature (Fig. 5g). Surprisingly,
307 although brain infiltrating CD4 T cell numbers did not change, these lymphocytes increasingly
308 assumed a Th1 phenotype with increased expression of IFN-γ when K^b was ablated on
309 endothelium (Fig. 5h). In a parallel set of experiments, we investigated whether antigen
310 recognition plays a role in infiltration and localization of IFN-γ producing CD8 T cells. We
311 infected mice and intravenously (IV) injected Alexa Fluor-488 conjugated anti-Thy1.2 antibody
312 3 minutes before euthanasia on day 6 of infection to label cells that have recently infiltrated brain
313 parenchyma from the bloodstream. It is important to note that K^b expressing Cre- mice are not
314 yet moribund on day 6 of infection. We also evaluated surface expression of CD11a as a

315 surrogate marker for cognate antigen-experienced CD8 T cells as previously described [28]. At 6
316 d.p.i. we show that numbers of Ag-experienced CD8 T cells were not different between K^b
317 expressing Cre- and Cdh5-Cre K^b cKO mice in meninges or cervical LNs of PbA infected mice.
318 However, numbers of brain infiltrated Ag-specific CD8 T cells were greatly reduced when K^b
319 was lost on vasculature (Fig.5i). K^b expressing Cre- mice presented with a significant increase of
320 CD11a+ CD8 T cells only in the IV- group, indicating that the majority had infiltrated the brain
321 prior to IV labeling. In Cdh5-Cre K^b cKO mice lacking K^b on vessels, numbers of both IV- and
322 IV+ CD8 T cells were greatly reduced, demonstrating that recognition of peptides presented by
323 K^b is required for optimal CD8 T cell infiltration (Fig. 5j). It is known that IFN-γ producing CD8
324 T cells have enhanced Ag-specific contacts, cytolytic killing and kinetics through paracrine and
325 autocrine IFN-γ signaling[29]. We therefore employed IV labeling to determine the localization of
326 IFN-γ producing CD8 T cells 6 d.p.i with PbA. We noted a slight trend towards increased
327 frequency of IFN-γ producing CD8 T cells in the recently infiltrated IV+ population in both Cre-
328 and Cre+ animals. However, this difference did not reach significance (Fig5k).
329 We next assessed the immune profile of the brains of D^b expressing mice in ECM.
330 Tissues were harvested at moribund, days 6-8 of infection. We observed no difference in the
331 overall numbers of CD45+ immune cells in the brain between D^b expressing Cre- and Cdh5-Cre
332 D^b cKO mice (Supplementary Fig. 6e). Surprisingly, we observed no change in CD8 T cell
333 infiltration between the groups, and numbers of CD4 T cells in the brain were also unchanged
334 (Fig. 5l-o). Expression of trafficking and adhesion molecules on CD8 T cells were assessed and
335 levels of CXCR3 and CCR7 were not significantly different between D^b Cre- littermates and
336 Cdh5-Cre D^b cKO (Supplementary Fig. 6j-m). Although overall brain infiltration of CD8 T cells
337 was unchanged, these lymphocytes presented with reduced IFN-γ production when D^b was

338 ablated on vasculature (Fig. 5p). In contrast, no change in CD4 T cell IFN-γ production was
339 observed (Fig. 5q). When assessing the role of Ag-recognition in infiltration, we observed 6
340 d.p.i. that numbers of CD11a+ Ag-experienced CD8 T cells were not different between Cre- and
341 Cdh5-Cre D^b cKO mice in meninges or cervical LNs. However, numbers of brain infiltrating
342 CD11a+ Ag-experienced CD8 T cells were significantly reduced when D^b was lost on
343 vasculature (Fig. 5r). We observed that numbers of previously infiltrated, IV- Ag-experienced
344 CD8 T cells were much lower in D^b Cre- mice than in K^b Cre- mice, although the IV+
345 populations between Cre-s were more comparable on day 6 of infection (Fig. 5j and 5s). This
346 suggests that Ag-specific CD8 T cell infiltration may begin at a later timepoint and escalate more
347 quickly with D^b on endothelium in comparison to K^b. Alternatively, we may not see a difference
348 between IV- and IV+ if vascular leakage is present as this could result in increased antibody
349 staining in the parenchyma (Fig. 5s). The previously infiltrated, Ag-experienced CD8 T cells in
350 the D^b Cre- littermates were significantly increased only when compared to the IV+ population
351 in the D^b cKO mice (Fig. 5s).

352 It is important to highlight that total numbers of brain infiltrated CD8 T cells are similar
353 between Cre- littermates (with either K^b or D^b) at endpoint (Fig. 5f and 5o). However, Ag-
354 experienced CD11a+ CD8 T cell numbers were much higher in K^b expressing than in D^b
355 expressing Cre- controls (Fig. 5i and 5r). As per localization of IFN-γ producing CD8 T cells, D^b
356 expressing Cre- animals had significantly increased frequency of CD8 T cells producing IFN-γ
357 in the IV labeled population on day 6 of infection, suggesting these cells have increased effector
358 function when recently infiltrated from vasculature (Fig. 5t). Meanwhile, Cdh5-Cre D^b cKO
359 animals had no change in frequency of IFN-γ producing CD8 T cells between IV+ and IV-
360 groups (Fig. 5t).

361 To further interrogate infiltration, we compared rates of entry of Ag-experienced
362 (CD11a+) and Ag-inexperienced (CD11a-) CD8 T cells on day 6 of infection. We observed that
363 CD11a+ Ag-experienced CD8 T cells in mice with K^b or D^b expression had faster infiltration
364 than mice with conditional deletion of class I molecules on endothelial cells, though this did not
365 reach significance in D^b cKO mice (Supplementary Fig. 6n-o). CD8 T cells that were CD11a-
366 (Ag-inexperienced) in K^b expressing mice had low rates of infiltration and there was not a
367 significance difference in infiltration between K^b Cre- and Cdh5-Cre K^b cKO mice
368 (Supplementary Fig. 6p). These data suggest that K^b class I molecule is important for Ag-specific
369 CD8 T cell brain infiltration in ECM. Although no differences were seen in CD11a- Ag-
370 inexperienced CD8 T cell rates of entry in between Cre- and D^b cKO mice, D^b expressing Cre-
371 mice rate of CD11a- CD8 T cell entry was double that of K^b expressing Cre- animals
372 (Supplementary Fig. 6p and q). Importantly, the same number of activated IFN-y producing CD8
373 T cells end up in the brain of K^b and D^b Cre- littermates at endpoint despite numbers of CD11a+
374 Ag-experienced CD8 T cells in D^b expressing mice being much lower on day 6 (Fig. 5g and p).
375 This demonstrates that D^b class I molecule on endothelium is required to initiate IFN-y
376 production by CD8 T cells to the same extent as K^b, and that each class I molecule on
377 endothelium differentially modulates the timeline of entry of Ag-specific CD8 T cells.
378 It is known that most neuropathology and vascular leakage during CM and ECM localize
379 to three distinct regions of the brain; olfactory, hippocampus and brainstem[16]. We therefore
380 wanted to assess whether infiltrating CD8 T cells enter brain parenchyma in these regions. Using
381 2-photon and confocal microscopy, we imaged cell dynamics and performed
382 immunofluorescence staining on brain tissues at late stages of infection. At 6-7 dpi we observed
383 CD8 T cells extravasating via post-capillary venules and entering regions of brain parenchyma in

384 K^b expressing Cre- mice (Supplementary Video 5). In K^b expressing Cre- littermates, we
385 observed parenchymal CD8 T cells in olfactory, brainstem, and hippocampal regions. However,
386 when K^b is deleted on vasculature, CD8 T cell infiltration into these regions is greatly decreased
387 (Supplementary Fig. 6r). When imaging D^b expressing Cre- littermates, we saw CD8 T cell
388 infiltration into brain parenchyma (Supplementary Video 6). We also confirmed that when D^b
389 expression is ablated on vasculature, CD8 T cells are still present in brain parenchyma in these
390 three regions (Supplementary Fig. 6s). These data support the findings of our spectral flow
391 cytometry data and demonstrate that CD8 T cells are infiltrated into regions of the brain affected
392 by ECM, except specifically when K^b is deleted on brain vasculature.
393
394 **Blood-brain barrier disruption is dependent on MHC Class I molecule expression by brain**
395 **endothelium.** Next, we assessed the contribution of discrete class I molecules on modulating
396 BBB disruption during ECM. At 6-8 dpi with PbA, mice were administered gadolinium I.P. and
397 evaluated for vascular permeability in the brain using T1-weighted gadolinium enhanced MRI.
398 In Cre- mice with K^b class I molecule expression intact, we see significant enhancement in
399 regions of olfactory bulb, brainstem and hippocampal regions periventricular to the lateral
400 ventricles (Fig 6a). All areas of leakage were assessed utilizing 3D volumetric analysis with
401 Analyze Software as previously described[16]. Brain vascular integrity was retained, and
402 gadolinium leakage was not observed when K^b expression was ablated on vasculature (Fig. 6a-
403 c). As a secondary method of vascular leakage assessment, we IV injected ~66 kDa FITC-
404 albumin, one hour prior to tissue harvest. FITC-albumin mean fluorescence intensity was
405 quantified in our three brain regions of interest. Uninfected and infected wildtype C57BL/6 mice
406 were included as visual reference controls (Fig. 6d). Cre- littermates with K^b expression had

407 significant FITC-albumin leakage in regions of olfactory bulb and brainstem. In contrast, Cdh5-
408 Cre K^b cKO animals lacking K^b on vasculature had negligible BBB disruption, indistinguishable
409 from uninfected controls (Fig. 6d). FITC-albumin leakage is quantified in Fig. 6e. PbA infected
410 D^b expressing Cre- Littermates presented with even more pronounced gadolinium-enhancement
411 in regions of interest than K^b expressing Cre- mice as measured by small animal MRI (Fig. 6a-c
412 and 6f-h). Cdh5-Cre D^b cKO mice however, presented with an intact blood brain barrier, with no
413 notable pathology when D^b is lost on vasculature during infection (Fig. 6f-h). In a secondary
414 analysis utilizing FITC-albumin leakage, we observed increased FITC-albumin mean
415 fluorescence intensity in D^b expressing Cre- olfactory bulb and brainstem (Fig. 6i-j). In Cdh5-
416 Cre D^b cKO mice, brain vascular integrity was retained, and no FITC-albumin leakage was
417 observed (Fig. 6i-j). Tight junction proteins are known to be downregulated in regions of BBB
418 disruption[16]. In human endothelial cells exposed to *Plasmodium falciparum* prbcs *ex vivo*, we
419 observed negative enrichment scores consistent with downregulation of tight junction proteins
420 (Supplementary Fig. 7a). We next performed Claudin-5 staining in our K^b and D^b models,
421 interrogating the regions of vascular leakage in the brains, where T cells were also observed to
422 infiltrate (Supplementary Fig. 8r-s). We saw that the vessels in regions of leakage and CD8 T
423 cell infiltration in both K^b and D^b Cre- littermates had a more sparse and punctate staining for
424 Claudin-5, indicating tight junction protein alteration (Supplementary Fig. 7b-c). However, K^b
425 and D^b cKO animals lacking class I molecules on vasculature had intact Claudin-5 expression
426 along vessels, despite the CD8 T cell infiltration seen in the Cdh5-Cre D^b cKO mice
427 (Supplementary Fig. 7b-c). Overall, these results indicate that vascular leakage and disruption of
428 BBB tight junctions occurs in mice via class I molecule restricted antigen presentation by brain
429 endothelium during *Plasmodium* infection.

430

431 **PbA infected parabionts sharing peripheral circulation demonstrate critical importance of**
432 **endothelial D^b expression to onset of ECM.** Previously, we had noted a decreased number of
433 activated CD8 T cells in inguinal LNs of PbA infected Cdh5-Cre D^b cKO mice (Fig. 3p). In
434 order to further rule out peripheral immune perturbations and fully demonstrate that
435 neuropathology was dependent on CD8 T cell interactions with MBMECs, we performed
436 parabiosis (Fig. 7a). Surgery was performed to conjoin D^b expressing Cre- littermate controls
437 with Cdh5-Cre D^b cKO mice in order to exchange peripheral blood and circulating immune cells.
438 Three weeks of healing and acclimation were observed before both mice were I.P. injected with
439 PbA to induce ECM (Fig. 7b). Our analysis revealed that all peripheral immune activation was
440 similar in the spleen and inguinal LNs of parabionts after infection (Fig.7c-d). In the brain, no
441 differences in CD45+ immune cell frequencies were observed and CD8 and CD4 T cell numbers
442 mirrored that of the previous mouse cohorts with no difference between groups (Fig. 7e). Also
443 consistent with prior cohorts, the Cdh5-Cre D^b cKO parabionts had decreased IFN-γ expression
444 by brain infiltrating CD8 T cells (Fig. 7e). We performed vascular permeability assays in our D^b
445 expressing Cre- to Cdh5-Cre D^b cKO parabionts and determined that the vascular leakage
446 phenotype was consistent with our previous data on D^b Cre- mice and had enhanced FITC-
447 albumin leakage. In contrast, despite having circulating immune cells from D^b expressing Cre-
448 mice, Cdh5-Cre D^b cKO mice resembled uninfected mice in that no vascular permeability was
449 detectable, directly supporting our previous data (Fig. 7f). This observation was further
450 supported by our results employing dual gadolinium enhanced T1-weighted MRI on the
451 parabionts. We observed diffuse enhancement throughout the brain of the Cre- parabiont,
452 indicating leakage. However, the conjoined Cdh5-Cre D^b cKO mice presented with no vascular

453 leakage as demonstrated by lack of gadolinium-enhancement with T1-weighted MRI and
454 retainment of FITC-albumin within vasculature (Fig. 7g). This data confirms that peripheral
455 immunity was not impeded and that changes in infiltration and activation status are truly barrier
456 and brain-specific and are impacted by class I restricted antigen presentation by MBMECs.
457
458 **Differential Endothelial Class I expression alters the neuroinflammatory profile of the**
459 **brain and targeted cell death during ECM.** To define downstream genes discretely regulated
460 by either K^b class I molecule or D^b class I molecule, we examined RNA transcriptomics data for
461 differentially regulated genes in PbA infected wildtype C57BL/6, K^b Cre-, Cdh5-Cre K^b cKO, D^b
462 Cre-, Cdh5-Cre D^b cKO, and uninfected controls of each group. We observed overlaps in gene
463 expression that were shared between wildtype C57BL/6 mice (with K^b and D^b) and K^b Cre- mice
464 (K^b only) (Fig. 8a). Gene programs regulated by K^b were genes primarily expressed in anti-
465 inflammatory A2 astrocytes, primed microglia, and cytokine and interferon signaling (Fig 8a and
466 Supplementary Table 3). Cdh5-Cre K^b cKO mice had very few differentially regulated genes,
467 similar to uninfected mice (Supplementary Figure 8a-c). We also noted distinctively differential
468 expression of genes that overlap between wildtype (with K^b and D^b) and D^b Cre- mice (D^b only)
469 (Fig. 8a). Gene programs regulated by D^b Cre- mice were indicative of a pro-inflammatory A1
470 astrocytic response, stage 2 damage-associated microglia, and microglial neurodegenerative
471 phenotype signatures[30, 31, 32, 33] .We also noted upregulation of genes associated with enhanced
472 Ag-presentation and cytotoxic T cell responses in the brains of these animals, indicating a strong
473 T cell response in these animals (Fig. 8a and Supplementary Table 3). Cdh5-Cre D^b cKO mice
474 had very few differentially regulated genes (Supplementary Figure 8d-f). Overall, the differential

475 gene expression observed between mice expressing distinct class I molecules further supports the
476 independent roles each class I contributes to this pathology.

477 We next wanted to determine what cells are being targeted by infiltrating CD8 T cells
478 during PbA infection. We infected mice with PbA and harvested tissue early on day 6 before all
479 mice were moribund. Brains were harvested to stain with a panel of antibodies to detect stages of
480 cell death. In K^b expressing Cre- littermates, we observed no significant increases in cell death of
481 MBMECs on day 6 of infection and no differences when K^b is deleted on vasculature (Fig. 8b).
482 When assessing neuronal cell death however, there were increased frequencies of cells with early
483 apoptotic markers, but complete neuronal cell death was not detectable by flow at this time.
484 There were no differences between K^b expressing Cre- littermates and Cdh5-Cre K^b cKO mice
485 (Fig. 8c). The low levels of endothelial and neuronal cell death may be attributed to the fact that
486 pathology is delayed in K^b mice in comparison to D^b mice. The K^b Cre- mice have average
487 clinical scores of ~1.5 on day 6 for ECM neurological signs, whereas D^b Cre- mice have average
488 clinical scores of >3 day on 6 (Fig. 8d and 8h). This delay in pathology may also translate to a
489 delay of neuronal and/or endothelial cell targeting as well. To examine this, we performed
490 another experiment in which all mice were allowed to progress to humane endpoint.
491 Transcriptomics analysis revealed that neurons do activate cell death pathways at this late
492 timepoint in K^b Cre- littermates (Fig. 8j). No endothelial cell death pathway activation was
493 noted. Cdh5-Cre K^b cKO mice had significantly improved clinical scores when K^b on
494 vasculature was deleted (Fig. 8d). In extended survival studies, we observed nearly complete
495 survival of Cdh5-Cre K^b cKO mice in comparison to Cre- littermate controls (Fig. 8e).

496 When assessing D^b mouse cohorts at day 6, we observed a striking increase in MBMEC
497 cell death in Cre- littermates that have D^b in comparison to Cdh5-Cre D^b cKO mice (Fig. 8f). A

498 significant increase in neuronal cell death was observed in D^b expressing Cre- littermates in
499 comparison to Cdh5-Cre D^b cKO mice (Fig. 8g). Similar to our observations in K^b, we observed
500 increased frequency of neurons with early apoptotic markers in the Cdh5-Cre D^b cKO mice, but
501 not late-stage neuronal death (Fig. 8g). These data were in agreement with transcriptomics data
502 showing activation of cell death pathways only in D^b Cre- mice (Fig. 8j). In an extended survival
503 study, mice with deletion of D^b on vasculature presented with striking improvement in clinical
504 scores and overall survival (Fig. 8h-i). Overall, neuronal cell death related gene expression was
505 increased in infected wildtype C57BL/6, K^b expressing Cre- mice and D^b expressing Cre- mice
506 (Fig. 8j). These studies demonstrate that class I molecule expression by endothelium is required
507 for the onset of neuronal cell death in the ECM model and that MBMECs undergo cell death late
508 in pathology following D^b MHC Class I-specific-CD8 interactions at vasculature.
509

510 **Discussion**

511 The role of Ag-presentation by brain endothelium and the effect on the CD8 T cell
512 effector response as a putative mechanism of CM have been highly debated in the cerebral
513 malaria field[3, 25, 34]. However, the role of individual class I molecule presentation by MBMECs to
514 brain infiltrating CD8 T cells has never been directly tested *in vivo*. In this study, we demonstrate
515 that targeted deletion of either K^b or D^b class I molecule on endothelium results in reduced T cell
516 interactions at brain vasculature and subsequently attenuated BBB disruption and
517 neuropathology. Comparisons to human data supports these findings, as well as other recent
518 studies which highlighted the importance of CD8 T cell interactions at the vasculature in the
519 development of CM and ECM[11, 17]. Overall, peripheral infection and all immune responses
520 develop normally in our mice, with the exception of mild decrease in CD8 T cell activation

521 marker CD44 at baseline in non-brain draining inguinal lymph nodes in Cdh5-Cre K^b cKO mice.
522 However, this difference resolves during infection. In Cdh5-Cre D^b cKO animals there was also
523 a slight decrease in the CD8 T cell activation marker CD44 in non-brain draining inguinal lymph
524 nodes during PbA infection. We addressed the potential effects these differences could pose in
525 ECM by performing parabiosis, which efficiently equalizes peripheral immune responses.
526 Endothelial cell-specific deletion of class I molecule was still protective, effectively ruling out
527 potential peripheral immune perturbations as having a role in protection from ECM.
528 CD8 T cells have been observed to interact with brain vasculature during
529 neuroinflammation[17, 26, 35, 36, 37]. However, few of these molecular interactions have been
530 successfully interrogated. The most well-characterized of these interactions is the CD8 T cell
531 slowing, rolling, and arrest on brain endothelium[38, 39, 40, 41, 42]. Using intravital microscopy on live
532 mice 6-7 dpi with PbA, we observe high numbers of T cells in both K^b and D^b expressing Cre-
533 littermates exhibiting slowing, rolling and arresting. In contrast, we observed a drop in these T
534 cell interactions with brain vasculature with the loss of either K^b or D^b class I expression by
535 endothelial cells. The novelty of these findings, however, lies in the fact that the adhesion
536 molecule expression is completely unchanged between Cre- and Cre+ animals in the K^b model.
537 This implies that the complete loss of T cell interactions we visualize by 2-photon are dependent
538 on the T cell-K^b class I interaction and not adhesion molecules. In D^b expressing Cre- mice, we
539 observe upregulation of P-selectin on brain endothelium. Surprisingly, despite their essential role
540 in T-cell rolling in vasculature, absence of E or P-selectin in mice have been experimentally
541 shown to be unnecessary for T-cell entry into the CNS, suggesting that T cell rolling is not
542 required for T-cell migration across inflamed BBB [39, 40, 41, 42]. However, most studies focusing on
543 diapedesis interrogated CD4 T cell interactions. ICAM-1 and VCAM-1 on endothelium was not

544 altered when class I molecules were ablated on vascular endothelial cells. Interestingly, when
545 either class I molecule was deleted on endothelium, expression of MHC Class II molecules was
546 found to be elevated. This may be a compensatory mechanism employed by endothelial cells in
547 order to establish a more robust CD4 T cell response when the CD8 T cell response is
548 impaired[43]. The ability of brain endothelium to shift the T cell effector response in the brain is in
549 agreement with several studies which propose that endothelial cell Ag-presentation may have
550 important immunomodulatory functions[35, 36, 37, 44].

551 Observing that deletion of both K^b and D^b class I molecule on endothelial cells resulted in
552 loss of T cell interactions with brain vasculature, we expected this may result in loss of CD8 T
553 cell infiltration. Interestingly, we observed differential CD8 T cell infiltration into brain
554 parenchyma. In Cdh5-Cre K^b cKO mice, we saw a reduction of CD8 T cells infiltrating the brain.
555 However, in Cdh5-Cre D^b cKO mice, we saw no changes in CD8 T cell infiltration, indicating
556 that overall CD8 T cell infiltration and D^b-restriction may be uncoupled in this model. Although
557 the deletion of D^b does not seem to affect overall infiltration of CD8 T cells, lack of D^b does alter
558 effector status. It is known that PbA strain of *Plasmodium* causes brain specific sequestration of
559 prbcs and activation of brain microvasculature[25]. However, work describing the PbA antigenic
560 D^b-restricted peptide SQLLNAKYL showed that when mice are infected with strains of
561 *Plasmodium* that do not cause adherence of prbcs to brain endothelium, CD8 T cells still entered
562 the brain but were not activated, resulting in absence of neurological symptoms in these
563 animals[45]. This supports our findings that when *Plasmodium* initiates endothelial cell Ag-
564 presentation, D^b is required for activation of CD8 T cells, but not infiltration during infection.
565 Furthermore, CD8 T cell TCR binding to cognate peptide presented by both H-2K^b and H-2D^b
566 on brain endothelium resulted in IFN-γ production by infiltrating CD8 T cells, which in turn,

567 caused differentially regulated cell death and mortality of the animal. This is supported by other
568 works showing that IFN-γ production induces a cascade to recruit more CD8 T cells to the
569 brain[43, 45, 46]. Overall, we demonstrated that endothelial K^b class I molecule interactions with
570 CD8 T cells is important for infiltration and activation, while endothelial D^b class I molecule
571 interactions activate CD8 T cells but does not influence diapedesis into parenchyma.

572 Previous work from our lab and others has hinted at the importance of antigen-specificity
573 of these infiltrating CD8 T cells in ECM neuropathology[16, 25, 45, 47]. However, definitive support
574 for this has been elusive and incomplete[17, 45 48]. Studies with transgenic parasites bearing model
575 epitopes are unable to recapitulate the complexity of the diverse CD8 T cell responses against the
576 wide array of native malaria Ags seen in mice and humans[49]. The epitopes that are known have
577 been shown to elicit variable CD8 T cell responses[49]. Although epitope discovery continues to
578 be an active area of research, there are currently only 83 known T cell epitopes for PbA out of
579 what is projected to be many thousands[35, 45, 50]. Importantly, a role for BBB damage-associated
580 molecular patterns (DAMPs) or parenchymal brain draining DAMPs in eliciting CD8 T cell
581 responses, have also not been ruled out[25, 34, 49, 50]. To date, our novel mouse models are the first
582 models capable of distinguishing between K^b and D^b class I restricted Ags specifically presented
583 by brain endothelial cells for interrogation of ECM pathogenesis. To assess the role of cognate
584 TCR-MHC interactions in CD8 T cell infiltration in this pathology, we used the well-established
585 surrogate marker strategy to track Ag-experienced CD8 T cells[28]. We saw no differences in Ag-
586 experienced CD8 T cells in the meninges or cervical LNs in either model. However, Ag-
587 experienced CD11a+ CD8 T cells were reduced specifically in brain parenchyma when lacking
588 K^b or D^b on vasculature[28, 51]. We also employed IV labeling of these infiltrating Ag-experienced
589 CD8 T cells 3 minutes prior to harvesting tissue. The caveat of this work is that IV labeling may

590 increase in parenchyma with increased vascular permeability, although this does not seem to be
591 the case in the K^b model. We saw that infiltration is much higher in K^b Cre- littermates than in
592 Cdh5-Cre K^b cKO mice at day 6, and that most CD8 T cells had previously infiltrated over time
593 prior to IV administration of labeling antibody. In the D^b model, however, we see comparable
594 amounts of IV labeled and IV negative cells in the brain indicating that a large influx of CD8 T
595 cells begins day 6 of pathology. These data suggest that K^b Ag-presentation by brain
596 endothelium tightly regulates activation and entry. However, D^b Ag-presentation by brain
597 endothelium does not employ as strict of regulation of CD8 T cell infiltration at the barrier. This
598 may mean that another predominant interaction, by a currently undefined cell type or chemokine
599 gradient, may be initiating this brain infiltration. This other interaction, however, does not
600 sufficiently activate the T cell as is seen when brain endothelium presents on D^b. Overall, these
601 data suggest that CD8 T cell activation and infiltration are influenced differentially in the D^b
602 model during ECM.

603 The chemokine receptor expression of activated T cells shows dynamic plasticity.
604 Several factors, including strength of antigenic signals, tissue-specific imprinting by priming
605 DCs, or cytokine milieu can influence the trafficking of T cells[52]. Both CXCR3 and CCR7 are
606 receptors on CD8 T cells shown to be necessary for recruitment into the brain to establish
607 ECM[24, 25, 26]. During ECM, olfactory bulb and brainstem are physically and functionally
608 damaged, with high prbc and leukocyte sequestration in these regions, which coincides with
609 vascular pathology and neuronal cell death[17, 27]. Specifically, the olfactory region has been
610 shown to highly upregulate CCL21, while brain endothelial cells highly express CXCL9 and
611 neurons highly express CXCL10[24, 27, 53]. Blocking their receptors CCR7 and CXCR3 results in
612 decreased CD8 T cell activation and recruitment to the CNS, respectively, as well as prolonging

613 survival during ECM[27, 54]. To support that T cells were sufficiently primed in the periphery and
614 imprinted for CNS-specific trafficking we examined chemokine receptor expression on CD8 T
615 cells trafficking to the brain. In the brain, frequency of CD8 T cells expressing CXCR3 and
616 CCR7, and MFIs of receptor expression were unchanged between Cre- and cKO animals in both
617 models; thereby reinforcing brain-specificity. The majority of data on CD8 T cell infiltration in
618 ECM focuses on the cortex, as this is the brain region most heavily infiltrated by CD8 T cells
619 during this pathology[55]. However, no prior reports have shown regional infiltration of areas
620 affected by vascular permeability. In this work we not only show regional CD8 infiltration to
621 areas with highest brain pathology, but that CD8 T cells are also present in regions without
622 vascular leakage, a topic previously debated[17].

623 CNS vascular leakage was prevalent in both K^b and D^b class I molecule expressing mice.
624 However, the presentation was distinct. In comparison to wildtype C57BL/6 animals, in which
625 both class I molecules are expressed, we saw less leakage in the midbrain of K^b expressing
626 animals, although there was still significant damage and leakage to olfactory and brainstem
627 regions. Alternatively, D^b expressing animals presented with worsened pathology, more closely
628 resembling that of the wildtype C57BL/6 mice which express both class I molecules.
629 Importantly, when either K^b or D^b were ablated specifically from vasculature, there was
630 complete rescue of vascular permeability. This finding is highly novel and strongly suggests that
631 antigens are being presented by either K^b or D^b class I molecules, specifically by brain
632 endothelial cells, to elicit distinct neuropathology associated with ECM. We also show that
633 Claudin-5 is altered in regions of permeability in Cre- animals, a known hallmark of vascular
634 pathology in this disease[16, 17]. However, animals lacking class I on vasculature preserved normal
635 Claudin-5 expression in the regions of interest.

636 We observed that K^b and D^b Ag-specific activation of recently infiltrated CD8 T cells
637 expressing IFN-γ correlates with differential vascular permeability in ECM. We therefore wanted
638 to interrogate whether K^b and D^b class I molecules produced differential activation of
639 neuroinflammatory pathways. We did observe distinct patterns of neuroinflammation, with
640 differential activation of astrocytes and changes in microglial and T cell activation states. This
641 may explain why D^b restricted Ag-presentation on endothelium, though resulting in later
642 infiltration of Ag-experienced CD8 T cells than K^b restriction on day 6, still resulted in stronger
643 T cell signaling, more cell death and worsened vascular leakage and survival at endpoint. Taken
644 together, these data indicate that discrete class I molecules on brain endothelium have
645 immunomodulatory capacity, capable of altering the neuroinflammatory profile of the brain
646 during ECM.
647 Knowing that K^b-restriction and D^b-restriction incite differential neuroinflammatory
648 profiles in the brain during PbA infection, we next sought to determine whether cellular targets
649 of the CD8 T cells were also distinct. We demonstrated that 6 dpi, mice with K^b class I
650 molecules displayed no markers of apoptosis or cell death in vascular endothelium. However,
651 neurons had early apoptotic markers and transcriptomic data supported that neuronal death is
652 induced at endpoint. When K^b was deleted from vasculature, endothelial cells were unchanged.
653 However, neurons no longer acquired the gene signature indicative of neuronal death. This data
654 suggests that CD8 T cell interactions with K^b-restricted Ag-presenting endothelial cells are not
655 required for targeted killing of MBMECs but are supportive of apoptotic neuronal cell death late
656 in pathology. The K^b-CD8 T cell interaction has been shown to modulate infiltration and
657 activation of CD8 T cells and may be involved in CNS reactivation or serve an imprinting role
658 which may instruct CD8 T cells to exact their effector functions in other ways or on other cell

659 types. When assessing D^b Cre- littermates, we observed a large percentage of cell death of
660 MBMECs which was ameliorated when D^b was deleted on vasculature. There was also an
661 increased percentage of cell death seen in neurons in D^b expressing Cre- animals which was
662 either resolved or delayed when D^b was lost on vasculature. This data demonstrates a
663 requirement for D^b-restricted Ag-presentation to CD8 T cells by the vasculature in order to enact
664 an effector response resulting in killing of both MBMECs and ultimately neuronal cell death.
665 The extent to which neuronal cell death is the result of direct killing by CD8 T cells, or through
666 alternative mechanisms has yet to be explored in these models. In previous work which detailed
667 CD8 T cell responses during ECM, they demonstrated that K^b and D^b are capable of presenting
668 similar peptides, though with very different binding affinities[49]. It is also known that receptor
669 affinities control effector responses and T cell polyfunctionality[45, 56, 57, 58, 59]. This is consistent
670 with our data showing that endothelial cells die when D^b presents, but not when K^b presents,
671 dependent upon the differential peptides they display as well as the strength of their interactions.
672 These results prove to be highly innovative as this is the first time that *in vivo* evidence has
673 directly shown the effects of K^b or D^b restricted Ag-presentation by brain endothelial cells during
674 ECM. Follow-up investigations should address direct mechanisms of cell death in more detail.
675 Alterations of cytokine milieu, the impact of vascular leakage and blood-derived factors on
676 neuroinflammation and CD8 T cell responsiveness still must be addressed.
677 In conclusion, our studies provide the first *in vivo* interrogation of the role of Ag-
678 presentation by individual class I molecules by MBMECs in developing ECM pathology. We
679 have dissected the contribution of both K^b and D^b to the onset of neuropathology and provide
680 evidence to support that K^b-restricted Ag engagement on endothelium plays a critical role in
681 CD8 T cell vascular adhesion, arrest, infiltration, and activation. These events in turn contribute

682 to blood-brain barrier tight junction downregulation, vascular leakage, and neuronal death.
683 Meanwhile, D^b-restricted Ag engagement on endothelium plays a role in vascular adhesion and
684 arrest but is inconsequential for CD8 T cell infiltration into brain parenchyma. However, the
685 interaction is important for CD8 T cell activation and IFN-γ secretion which is associated with
686 heightened CD8 T cell motility and toxicity, tight junction downregulation, and vascular
687 permeability[25, 29, 46, 60]. Strikingly, we show that only CD8 TCR recognition of D^b-restricted
688 antigens by brain vasculature results in killing of MBMECs and subsequent neuronal cell death.
689 We contend that these insights into the pathogenesis of cerebral malaria will provide rationale for
690 therapeutic targeting of these interactions. Anti-malarial drugs can serve to lessen parasite
691 burden, but show no improvement in neurological symptoms once there is brain involvement[17].
692 We therefore propose that patients with CM may benefit from endothelial-specific therapeutics
693 which serve to specifically blockade T cell-class I interaction in addition to standard-of-care anti-
694 malarial drugs.
695

696 **Methods**

697 **Animals.** Male and female C57BL/6J WT (stock no. 000664) and Cdh5-Cre mice (stock no.
698 033055) were purchased from Jackson Laboratory. H-$2K^b$ LoxP and H-$2D^b$ LoxP mice were
699 generated by our program as previously described, in the C57BL/6 background [61, 62]. H-$2K^b$
700 LoxP and H-$2D^b$ LoxP mice were crossed with Cdh5-Cre mice to generate Cdh5-Cre K^b cKO
701 and Cdh5-Cre D^b cKO mice that express Cre under the *Cdh5* promoter and undergo endothelial-
702 specific targeted gene deletion of H-$2K^b$ and H-$2D^b$ molecules. Mice were then bred and
703 maintained under specific pathogen free conditions at the Mayo Clinic Animal Facility. In the
704 studies, 15–20-week-old mice were used for all experiments with appropriate age and sex-

705 matched controls. All experiments were conducted in accordance with guidelines from the
706 National Institutes of Health and under the approval of the Mayo Clinic Institutional Animal
707 Care and Use Committee.
708
709 ***Plasmodium* infection.** *Plasmodium berghei* ANKA (PbA) stocks were generously provided by
710 J. Harty at the University of Iowa and S. Hamilton Hart at the University of Minnesota Medical
711 School. PbA infection was induced in 15–20-week-old mice via intraperitoneal injection of ~10^6
712 parasitized red blood cells on day 0. Mice were monitored twice daily until onset of clinical signs
713 were observed (days 6-8 post infection), and then continuously. Blinded scores were obtained
714 daily, scoring signs of neurological impairment until endpoint. Mice were ranked for clinical
715 signs of ECM adapted from Hortle et al[63]: 0, no clinical symptoms; 1, reduced movement and
716 limp/flaccid tail; 2, rapid breathing and transient hunching posture; 3, hunched, ruffled fur and
717 loss strength in four limb hang test; 4, severe disease (ataxia, seizures, coma); and 5, death.
718 Moribund animals were scored 4.5 and humanely euthanized. Mice were classified as having
719 ECM if displaying symptoms between days 6-8 post-infection. Peripheral parasitemia was
720 assessed using thin blood smears and Geimsa staining as outlined on the Centers for Disease
721 Control website and as previously described[64].
722
723 **Acute TMEV and TMEV-OVA Infection**
724 The Daniel's strain of TMEV was prepared as previously described[62]. TMEV-XhoI-OVA8
725 (TMEV-OVA) was generated and prepared by our group as previously described[23]. At 10-12
726 weeks of age, mice were anesthetized with 1-2% isoflurane and infected intracranially (i.c.) with
727 2 x 10^6 PFU (10µL) of the Daniel's strain of TMEV, or 2 x 10^5 PFU of TMEV-OVA. Virus was

728 delivered to the right hemisphere of the brain via automatic 1 mL Hamilton syringe (Hamilton
729 Company, Reno, NV). Mice were euthanized for high-dimensional flow cytometry of tissues at
730 7-days post infection (dpi).
731
732 **Magnetic resonance imaging (MRI).** MRI capture and analysis was conducted as previously
733 reported using Bruker Avance II 7 Tesla or Bruker Avance 16.4 Tesla vertical bore small animal
734 MRI system (Bruker Biospin, Billerica, MA)[65]. Gadolinium (Multihance-Bracco) was
735 administered intraperitoneally (100µL of 100mg/kg) ~15 minutes before scans. 25 mm and 34
736 mm volumetric coils were utilized. Animals were anesthetized with continuous isoflurane
737 administered through nose cone. Respiration and heart rate were monitored with an MRI
738 compatible vitals monitoring system (model 1030; SA Instruments, Stony Brook, NY).
739 After axial and sagittal tripilot positioning scans, isotropic 3D T1-weighted scans were employed
740 to detect gadolinium, with an approximate scan time of 30 minutes. Maximum intensity
741 projection scans were performed to detect gadolinium, with an approximate scan time of 10
742 minutes. Scoring was performed by two independent observers, blinded to genotype with <10%
743 intra-observer variation found. Analyze12.0 software (Biomedical Imaging Resource; Mayo
744 Clinic, Rochester, MN) was employed to analyze T1 data and to generate 3D maps of
745 gadolinium enhancement. Maximum intensity projection data was analyzed using Fiji Is Just
746 ImageJ (FIJI) 2.3.0; Java 1.8.0_172.
747
748 **Immunofluorescence**. Brains used for immunofluorescence staining were either fresh frozen or
749 paraformaldehyde fixed following mouse euthanasia and transcardial perfusion with ice-cold
750 PBS. Brains harvested after 2-photon imaging and FITC-albumin injection were harvested

751 without perfusion and paraformaldehyde fixed. All brain tissues were embedded in Tissue-Tek
752 OCT Compound, frozen on dry ice and sliced on cryostat with the exception of FITC-albumin
753 injected brains which were embedded in 4% agarose and sliced with vibratome. All brain slices
754 were mounted on SuperFrost Plus microscope slides and stored at 4 degrees.
755
756 **Single-cell suspension.** Mice were euthanized via isoflurane per IACUC guidelines and
757 transcardially perfused with ice-cold PBS. Brains and meninges were harvested and processed as
758 previously described[66, 67], via dounce homogenization and 30% Percoll gradient or enzymatically
759 digested using mouse tumor dissociation kit and gentleMACS™ Octo Dissociator (Miltenyi
760 Biotec). Spleens and lymph nodes were either digested with Collagenase IV/DNAse or not
761 digested before mechanical disruption. Lymph nodes were dissociated using frosted glass slides
762 and spleens were dissociated through 70 μM filter. Thymus samples were processed using
763 mechanical disruption through 70 μM filter. Blood was collected (100μl) into 1 mL heparin
764 (100U/mL). Spleens underwent ACK RBC lysis for 3 minutes and blood samples for 1minute.
765 All samples were filtered using 70 μM filters before counting, staining and running on flow
766 cytometer.
767
768 **Flow cytometry.** After resuspension in PBS, cells were either first stained with either Zombie
769 UV or Zombie NIR fixable viability dyes (BioLegend) (1:1000) for 20 minutes at room
770 temperature in the dark or Ghost Red 780 Viability dye (Tonbo) was added to surface stain
771 master mix. Samples underwent Fc-receptor block and staining for 30 minutes at 4 degrees with
772 surface staining antibodies. Panels requiring intracellular staining were then fixed and
773 permeabilized using Cyto-Fast™ Fix/Perm Buffer Set (BioLegend), and then stained with

774 intracellular antibodies for 30 minutes at room temperature in the dark before washing. All flow
775 panel staining was performed with this method with the exception of Annexin staining, which
776 required staining in Annexin V Binding Buffer (Invitrogen) for 15 minutes at room temperature
777 prior to fixation and permeabilization and intracellular staining. The antibodies that are specific
778 for surface markers included CD103 Brilliant Violet 421 (121422; BioLegend), NK1.1 Pac Blue
779 (108722; BioLegend), B220 Pac Blue (103227; BioLegend), CD62L Brilliant Violet 480
780 (746726; BD Biosciences), CD11b VioGreen (130-113-239; Miltenyi Biotec), CD44 Brilliant
781 Violet 570 (103037; BioLegend), CD80 Brilliant Violet 605 (104729; BioLegend), Ly6C
782 Brilliant Violet 650 (128049; BioLegend), H-2K^b/H-2D^b Brilliant Violet 750 (746869; BD
783 Biosciences), CCR7 Brilliant Violet 785 (120127; BioLegend), I-A/I-E BB515 (565254; BD
784 Biosciences), CD8a Spark Blue 550 (100780; BioLegend), CD45 PerCP (103130; BioLegend),
785 Ly6G PerCP-eFluor 710 (46-9668-82; Invitrogen), OX40L PE-Dazzle 594 (108816;
786 BioLegend), CD40 PE-Cy5 (124618; BioLegend), CD31 PE-Cy7 (25-0311-82; Invitrogen), CD3
787 Spark NIR 685 (100262; BioLegend), CD11c Alexa Fluor 700 (117320; BioLegend), CD4 APC-
788 Fire 750 (100568; BioLegend), CD25 Brilliant Violet 421 (102034; BioLegend), TCRβ APC
789 (20-5961-U100; Tonbo biosciences), c-kit Brilliant Violet 786 (564012; BD Biosciences), CD69
790 Brilliant Violet 650 (740460; BD Biosciences), Ly51 FITC (108305; BioLegend), EpCAM PE-
791 Cy7 (118216; BioLegend), CD8a Pac Blue (563898; BD Biosciences), CD4 APC (100516;
792 BioLegend), CD11a PE (141006; BioLegend), CD16/CD32 (553141; BD Pharmingen), Thy1.2
793 Alexa Fluor 488 (105316; BioLegend), I-A/I-E Pac Blue (107620; BioLegend), CD8a Brilliant
794 Violet 510 (100751; BioLegend), CD44 Brilliant Violet 650 (740455; BD Biosciences), Ly6G
795 Brilliant Violet 711 (46-9668-82; Invitrogen), CD4 Brilliant Violet 786 (563727; BD
796 Biosciences), Ly6C PerCP (128027; BioLegend), CD45 PE-CE594 (562420; BD Horizon),

797 CD11b PE-Cy5 (55-0112-U100; Tonbo biosciences), TCRβ PE-Cy7 (60-5961-U100; Tonbo
798 biosciences), B220 Spark NIR 685 (103268; BioLegend), CD62L APC-Fire 750 (104450;
799 BioLegend), CD11c Brilliant Violet 605 (117333; BioLegend), Annexin V(25-8103-72;
800 Invitrogen), B220 APC-Fire 810 (103277; BioLegend), CD26 Brilliant Violet 605 (745125; BD
801 Biosciences), CD80 Brilliant Violet 711 (104743; BioLegend), I-A/I-E Brilliant Violet 786
802 (743875; BD Biosciences), CD8a Brilliant Violet 421 (563898; BD Biosciences), CD31 APC-
803 Fire 750 (102528; BioLegend), CD11a PE-Cy7 (101122; BioLegend), CD31 PE-Dazzle
804 (102526; BioLegend), CXCR3 Brilliant Violet 421 (126521; BioLegend), CD106 Alexa Fluor
805 647 (105712; BioLegend), CD62P PE (148306; BioLegend), CD54 Brilliant Violet 711 (116143;
806 BioLegend), CD8 Brilliant Violet 570 (100740; BioLegend), Zombie NIR viability dye (Cat.
807 #423105; BioLegend), Zombie UV (423107; BioLegend). To assess cytokine production cells
808 were stained with intracellular markers after fixation and permeabilization: NeuN APC (100920;
809 Novus), IFNγ Brilliant Violet 785 (563773; BD Biosciences), IFNγ APC (20-7311-U100; Tonbo
810 biosciences) IL-12 PE (505204; BioLegend), IFNγ PE (50-7311-U100; Tonbo Biosciences). In
811 noted experiments, intravenous injection of 2ug of Thy1.2 Alexa Fluor 488 were administered 3
812 min. before collecting tissues to label T cells in vasculature. All samples were acquired on Cytek
813 Aurora spectral flow cytometer (Cytek, Fremont, CA). All analysis was performed using FlowJo
814 software version 10.8.1(FlowJo LLC, Ashland, OR).
815
816 ***In vivo* two-photon microscopy.** Mice were intravenously injected with 2 μg of Thy1.2 Alexa
817 Fluor 488 just prior to cranial window surgery, approximately 30 min prior to imaging. Cranial
818 windows were implanted as described [68 69]. In brief, under isoflurane anesthesia (3% induction,
819 1.5–2% maintenance), a circular craniotomy (<5 mm diameter) was made over somatosensory

820 cortex with the center at about -2.5 posterior and +2 lateral to bregma. A circular glass coverslip
821 (5 mm diameter, Warner) was secured over the craniotomy using dental cement (Tetric
822 EvoFlow). A four-point headbar (NeuroTar) was secured over the window using dental cement.
823 Mice were injected intravenously with intravascular dye 70,000 MW Dextran-Texas Red
824 (Invitrogen, D1830) 5 minutes before imaging. Alexa Fluor 488 (T cells) and Dextran-Texas
825 Red (vessels) were excited by a tunable Ti:Sapphire Mai Tai DeepSee laser (Spectra Physics,
826 CA, USA) at 940 nm and the emission was collected at 525/50 and 630/75 nm, respectively (U-
827 MF2, Olympus, Japan). An Olympus LUMPLFLN 40x water-immersion objective was used to
828 acquire image stacks. A 30-μm stack with 2 μm z-resolution and 512 × 512 pixels were acquired
829 every minute for a period of 10-30 min. Images were analyzed by Fiji ImageJ [70]. To analyze T
830 cell velocity, each 30-μm stack was first aligned along the z axis using the StackReg plugin
831 (Rigid Body) and Z-project into one image. Then images of every minute were stacked and
832 aligned using StackReg plugin (translation). The T cell velocity was measured using the Manual
833 Tracking plugin tracing for 10 min per field. The arrest coefficient is the percentage of each track
834 that a cell is immobile (instantaneous velocity <2 μm/min) [71].
835
836 **Parabiosis:** Procedure was performed as previously described. In brief, two female age-matched
837 mice of similar weight were selected. Mice were either littermates or co-housed for two weeks
838 prior to surgery. Anesthesia was induced and maintained with Ketamine/Xylazine (100/10
839 mg/kg; maintenance dose 30/3 mg/kg). Opthalmic ointment was placed on eyes. Mice are tested
840 for reflex responses to ensure anesthetic depth. For analgesia during surgery, we administered
841 Carprofen and Buprenorphine-SR subcutaneously (5 mg/kg and 1 mg/kg). Animals were shaved
842 on the flank and prepped for surgery with Betadine swabs and sterile drapes. Using a sharp

843 scissor, superficial epidermal incision was continuously made along the flank starting at 0.5 cm
844 rostral of olecranon to 0.5 cm superior to patella. Skin absorbable 3-0 silk suture were used to
845 join elbow and knee joints (Ethicon Inc, Somerville, NJ). Simple continuous suture was
846 performed with absorbable 4-0 vicryl suture (Ethicon Inc, Somerville, NJ) for closer of incision.
847 Post-operatively we administer 1 ml of 0.9% NaCl fluids subcutaneous, analgesics Carprofen
848 intraperitoneally and Buprenorphine SR subcutaneously. Mice were placed on heating pad and
849 observed for a minimum of 3 hours after surgery. Prophylactically, mice were treated with
850 antibiotic Enrofloxacin (50 mg/kg) 10 days post-operatively. Parabiont pairs underwent a
851 minimum of 3 weeks of healing and acclimation time before experimental use. Procedure was
852 performed according to the IACUC guidelines at Mayo Clinic.
853
854 **Nanostring**. Brain dissections were subjected to RNA extraction (Qiagen RNAeasy Mini Kit Cat.
855 No. 74104), followed by nanodrop concentration and purity analysis. RNA samples were applied
856 to NanoString nCounter (NanoString Technologies, Seattle, WA) digital RNA quantification,
857 using the predesigned mouse Glial Profiling Panel codeset. The Glial Profiling Panel reagents were
858 provided by Nanostring. Reporter CodeSet Lot#RC8131X1. Capture Codeset Lot#CP8131X1.
859 Nanostring analysis was performed by the Thompson Lab at the Mayo Clinic Comprehensive
860 Cancer Center at Mayo Clinic Florida. Briefly, 100 ng of total RNA was hybridized to capture-
861 reporter probe codesets and immobilized on NanoString cartridges. Excess RNA and probes were
862 removed, and digital barcodes were counted. NanoString nCounter analysis software (v4.0) was
863 used for counting, quality control, and normalization. Transcript counts were normalized
864 according to NanoString's recommendations. Normalization parameters were applied with
865 normalization cutoff of 10. All samples were quality checked for quality and concentration. 13

866 housekeeping genes, 6 positive control genes, and 8 negative control genes were utilized for
867 normalization.
868
869 **Human brain microvascular endothelial cells**
870 Human brain endothelial cell microarray data available through public repository at Gene
871 Expression Omnibus (GEO), accession number GSE9861. Outlined in the publication by Tripathi
872 et al, HBMECs were isolated from human brain specimens and characterized as described
873 previously[19, 72]. In brief, HBMECs (passage < 6) from single adult donor were used for the biologic
874 replicate experiments. For microarray experiments, HBMECs were grown in collagen-coated 6-
875 well plates until cells achieved about 80% to 90% confluence. The medium was then changed to
876 RPMI 1640 with 5% fetal bovine serum for 24 hours before coincubation with Pf-IRBCs, at which
877 time HBMECs are confluent. Endothelial cells mycoplasma infection negative (Vector
878 Laboratories).
879
880 **Gene Expression Analyses.** Human microarray data with accession number GSE9861[19] was
881 utilized via Gene Expression Omnibus (GEO), a public functional genomics data repository
882 supporting MIAME-compliant data submissions. Genes from human and mouse datasets were
883 identified to be differentially expressed from each in comparison to a control group using either
884 Ingenuity Pathway Analysis software (Qiagen), or Geo2R[73]. Gene set enrichment analysis
885 (GSEA) was also performed on human data[74].
886
887 **Statistics.** When comparing results from two groups, an unpaired Student's t-test was used.
888 When comparing results from two groups of paired mice, a paired Student's t-test was used.

When comparing results from three groups, a one-way analysis of variance (ANOVA) using Tukey's post-hoc multiple comparisons test was used. A two-way ANOVA when comparing statistically significant difference between the means of three or more independent groups that have been split on two variables, a two-way ANOVA using Šidák's multiple comparisons test was used. All statistical analyses were performed using Prism 6.0 (GraphPad Software) or Excel. Data are presented as the mean ± SD. and All p-values are shown or ns for non-significant p-value ($p > 0.05$).

Acknowledgments: We would like to thank Dr. Vanda Lennon for her feedback, Dr. Emma Goddery and Dr. Roman Khadka for discussions and Ryan Meloche for assisting with logistics of dual MRI. Some graphics were prepared on Biorender.com. Tetramers were provided by the NIH tetramer facility. **Funding sources:** R01NS103212 (AJJ), RF1NS122174 (AJJ), and F31NS116924 (CEF), R01AI167847 (JTH), Nanostring-Glial Panel Grant (CEF).

Financial disclosures: We have no financial interests to disclose.

914 Figure Legends

915

916 **Fig 1. Mouse and human brain microvascular endothelial cells become antigen presenting**
917 **cells during cerebral malaria** a) Flowchart showing steps of peripheral malaria infection,
918 development of experimental cerebral malaria and RNA extraction for Nanostring analysis. b)
919 Volcano plot of differentially expressed genes in whole brains of uninfected C57BL/6 mice
920 versus PbA infected mice on day 6 of infection. Significantly upregulated genes are indicated on
921 upper right (purple dots). Significantly downregulated genes are indicated on upper left
922 (turquoise dots). Horizontal dotted line indicates cutoff of adjusted p-values (-Log10 of adjusted
923 p-value 1.3 corresponding to a threshold of p-value of 0.05). Vertical dotted line indicates cutoff
924 of log2 Fold change (-1.5 to 1.5). c) Ingenuity Pathway Analysis (IPA) was performed, and
925 Causal network analysis identified MHC Class I family as the most significant network master
926 regulator in experimental cerebral malaria pathology which led to the differential expression of
927 the genes of interest. Depicted in c) a schematic of the homologous master regulator pathway and
928 corresponding downstream genes. Coloring of the molecules corresponds to calculated z-scores
929 (algorithm predicting activation or inhibition). Red indicates increased gene activation, orange
930 indicates predicted activation of pathways, green indicates decreased gene activation, blue
931 indicates predicted inhibition of pathways, white indicates a z-score of zero with equal evidence
932 for activation and inhibition, grey indicates that z-score could not be calculated. d) Canonical
933 pathway analysis identified significantly differential signaling pathways. P-value of overlap was
934 adjusted using the Benjamini-Hochberg correction method. Bars are arranged in order of
935 significance score with threshold (red line) set at p-value 0.05 (corresponding to a negative log
936 value of 1.3). Coloring of bars corresponds to calculated z-scores (algorithm predicting
937 activation or inhibition). Orange bars indicate activated pathways, blue indicates inhibited
938 pathways, white indicates a z-score of zero with equal evidence for activation and inhibition,
939 grey indicates that z-score could not be calculated. e) Schematic depicting C57BL/6 and naming
940 convention of mouse brain microvascular endothelial cells (MBMECs). High-dimensional flow
941 cytometry was performed on mouse brains on day 6 of PbA infection and uninfected age and sex
942 matched controls. f) Representative histogram of MHC Class I expression on MBMECs and
943 quantified frequency of MHC Class I high endothelial cells. g) Representative histogram of
944 MHC Class II expression on MBMECs and quantified frequency. h) Schematic depicting human
945 subjects and naming convention of human brain microvascular endothelial cells (HBMECs). i-j)
946 Box plots depicting Log_2 expression data from human endothelial cells in published microarray
947 (GEO Accession: GSE9861). i) MHC Class I Log_2 expression in control HBMECs vs.
948 *Plasmodium* exposed HBMECs. j) MHC Class I Log_2 expression in control HBMECs vs.
949 *Plasmodium* exposed HBMECs selected as highly activated (with high expression of adhesion
950 molecules). k) Log_2 Fold change of genes of interest which lie downstream of the MHC class I
951 signaling pathway in HBMECs during *Plasmodium* falciparum infection. GSEA was performed
952 on HBMEC transcriptomic data. l) Enrichment plot showing enrichment of molecular signature
953 for T cell activation involved in immune response pathway. The y-axis represents enrichment
954 score (ES) and on the x-axis are genes (vertical black lines) represented in gene sets. The green
955 line connects points of ES and genes. ES is the maximum deviation from zero as calculated for
956 each gene going down the ranked list and represents the degree of over-representation of a gene
957 set at the top or the bottom of the ranked gene list. The colored band at the bottom represents the
958 degree of correlation of genes with the phenotype (red for positive and blue for negative
959 correlation). Significance threshold set at nominal p-value < 0.05. Gene sets for T cell activation

960 involved in immune response were significant only in HBMECs during infection. Data were
961 analyzed with unpaired t test (f, g, i, and j). Box plots present the mean ± SD. All p-values are
962 shown or ns for non-significant p-value *(p > 0.05)*.
963
964
965
966 **Fig 2. Normal peripheral infection and immunity in mice with K^b class I molecule**
967 **conditionally ablated on vasculature** a) Schematic depicted Cre-LoxP strategy. Cdh5-Cre mice
968 were crossed to transgenic H-2K^b LoxP mice. b) Representative MFI plot comparing C57BL/6,
969 Cdh5-Cre K^b cKO, and Cre-Littermate expression of MHC I on brain endothelium in naïve mice.
970 c) Quantification of MHC I MFIs on brain endothelial cells using arbitrary units (A.U.) in naïve
971 mice. d) Percentage of brain endothelial cells expressing high levels of MHC Class I molecules
972 in naïve mice. e) Representative flow plot of C57BL/6, Cdh5-Cre K^b cKO, and Cre-Littermate T
973 cell subsets in thymus. f) Percentage of thymic T cell subsets. g) Schematic representing timeline
974 of infection for development of ECM. h) Representative MFI plot comparing C57BL/6, Cdh5-
975 Cre K^b cKO, and Cre-Littermate expression of MHC I on brain endothelium in PbA infected
976 mice. i) Quantification of MHC I MFIs on brain endothelial cells using arbitrary units (A.U.) in
977 PbA infected mice. j) Percentage of brain endothelial cells expressing high levels of MHC Class
978 I molecules in PbA infected mice. k) Percentage of granulocytes in spleens of infected mice. l)
979 Percentage of antigen-presenting cells in spleens of infected mice. m) Percent parasitemia
980 quantified by imaging Giemsa-stained thin blood smears in PbA infected mice. n) Representative
981 UMAPs depicting peripheral organs and immune cell populations and respective heats maps with
982 CD44 activation marker expression. o) The scatter plots show quantified absolute cell counts of
983 CD8 T cells, CD4 T cells and CD44hi CD8 T cells and CD4 T cells in the respective organs
984 depicted in n). Data were analyzed with unpaired t test or 2way ANOVA with multiple
985 comparisons. Scatterplots and bar plots present the mean ± SD. All p-values are shown or ns for
986 non-significant p-value *(p > 0.05)*.
987
988 **Fig 3. Normal peripheral infection and immunity in mice with D^b class I molecule**
989 **conditionally ablated on vasculature** a) Schematic depicted Cre-LoxP strategy. Cdh5-Cre mice
990 were crossed to transgenic H-2D^b LoxP mice. b) Representative MFI plot comparing C57BL/6,
991 Cdh5-Cre D^b cKO, and Cre-Littermate expression of MHC I on brain endothelium in naïve mice.
992 c) Quantification of MHC I MFIs on brain endothelial cells using arbitrary units (A.U.) in naïve
993 mice. d) Percentage of brain endothelial cells expressing high levels of MHC Class I molecules
994 in naïve mice. e) Representative flow plot of C57BL/6, Cdh5-Cre D^b cKO, and Cre-Littermate T
995 cell subsets in thymus. f) Percentage of thymic T cell subsets. g) Schematic representing timeline
996 of infection for development of ECM. h) Representative MFI plot comparing C57BL/6, Cdh5-
997 Cre D^b cKO, and Cre-Littermate expression of MHC I on brain endothelium in PbA infected
998 mice. i) Quantification of MHC I MFIs on brain endothelial cells using arbitrary units (A.U.) in
999 PbA infected mice. j) Percentage of brain endothelial cells expressing high levels of MHC Class
1000 I molecules in PbA infected mice. k) Percentage of granulocytes in spleens. l) Percentage of
1001 antigen-presenting cells in spleens. m) Percent parasitemia quantified by imaging Giemsa-
1002 stained thin blood smears in PbA infected red blood cells. n) Scatter plots show quantified
1003 absolute cell counts of CD8 T cells, CD4 T cells and CD44hi CD8 T cells and CD4 T cells in
1004 spleen. o) Scatter plots show quantified absolute cell counts of CD8 T cells, CD4 T cells and
1005 CD44hi CD8 T cells and CD4 T cells in peripheral blood. p) Scatter plots show quantified
1006 absolute cell counts of CD8 T cells, CD4 T cells and CD44hi CD8 T cells and CD4 T cells in

1007 inguinal LN. Data were analyzed with unpaired t test or 2way ANOVA with multiple
1008 comparisons. Scatterplots and bar plots present the mean ± SD. All p-values are shown or ns for
1009 non-significant p-value *(p > 0.05)*.
1010
1011 **Fig 4. T cell dynamics at brain vasculature are dependent on MHC class I expression**
1012 **during infection** a) Representative images of T cells in brain vasculature with blood vessels
1013 labeled with I.V. Dextran-Texas ~5 min. prior to imaging and T cells I.V. labeled with anti-
1014 Thy1.2-Alexa Fluor 488 ~30 min. Inset is representative of T cell tracking over time through
1015 acute cranial window on days 6-7 post PbA infection. T cells (green) were visualized interacting
1016 with blood vessels (red) over periods of 10-30 min. Upper row represents K^b Cre- littermates and
1017 bottom row represents Cdh5-cre K^b cKO mice. Scale bar, 10 µM. b) Scatter plot represents
1018 numbers of T cells visualized over 10 min time periods/FOV. c) T cell velocity was measured
1019 using the Manual Tracking plugin in FIJI. Data are representative of µm/min over periods of 10
1020 min per field and per cell. d) Percentage of T cells contacting vessels was calculated by obtaining
1021 the percent of all visualized T cells that contacted vasculature over many fields of view. Each
1022 data point is representative of the overall average percentage/mouse. e) The arrest coefficient
1023 is the percentage of each cell track that a cell is immobile (instantaneous velocity <2 µm/min).
1024 Each dot represents one cell and its percentage of contacts over time. (n = 5-7 mice per group).
1025 See corresponding S1-S5 movies. High-dimensional flow cytometry was performed to assess
1026 levels of protein expression on brain endothelium day 6 of PbA infection. f) Scatter plot
1027 represents MFI values of P-selectin on brain endothelial cells. g) MFI of ICAM-1on brain
1028 endothelial cells h) MFI of VCAM-1 on brain endothelial cells. i) Percentage and MFI
1029 quantification of MHC Class II molecules on brain endothelial cells with representative
1030 histogram. j) Representative images of T cells in brain vasculature labeled as described above.
1031 Inset is representative of T cell tracking over time through acute cranial window on days 6-7 post
1032 PbA infection. T cells (green) were visualized interacting with blood vessels (red) over periods
1033 of 10-30 min. Upper row represents D^b Cre- littermates and bottom row represents Cdh5-cre D^b
1034 cKO mice. Scale bar, 10 µM. k) Scatter plot represents numbers of T cells visualized over 10
1035 min time periods/FOV. l) T cell velocity was measured using the Manual Tracking plugin in
1036 FIJI. Data are representative of µm/min over periods of 10 min per field and per cell. m)
1037 Percentage of T cells contacting vessels was calculated by obtaining the percent of all visualized
1038 T cells that contacted vasculature over many fields of view. Each data point is representative of
1039 the overall average percentage/mouse. n) The arrest coefficient is the percentage of each cell
1040 track that a cell is immobile (instantaneous velocity <2 µm/min). Each dot represents one cell
1041 and its percentage of contacts over time. (n = 5 mice per group). See corresponding S1-S5
1042 movies. High-dimensional flow cytometry was performed to assess levels of protein expression
1043 on brain endothelium day 6 of PbA infection. o) Scatter plot represents MFI values of P-selectin
1044 on brain endothelial cells. p) MFI of ICAM-1on brain endothelial cells q) MFI of VCAM-1 on
1045 brain endothelial cells. r) Percentage and MFI quantification of MHC Class II molecules on brain
1046 endothelial cells with representative histogram. Data were analyzed with unpaired t test.
1047 Scatterplots and bar plots present the mean ± SD. All p-values are shown or ns for non-
1048 significant p-value *(p > 0.05)*.
1049
1050 **Fig 5. Modulation of individual class I molecules on brain endothelium results in brain-**
1051 **specific CD8 T cell infiltration changes.** a) BioRender schematic of events in the periphery
1052 leading up to cerebral malaria. b) Representative UMAP key, colorized to highlight the different

1053 cell subsets in the brain. c) Representative UMAPs of K^b Cre- Littermate and Cdh5-cre K^b cKO
1054 brains, colorized with heat map of CD8 expression. d) Pie charts with corresponding frequencies
1055 of cell subset in K^b Cre- Littermate and Cdh5-cre K^b cKO brains (of CD45+) e) Absolute counts
1056 of CD4 T cells in the brains of infected K^b Cre- Littermate and Cdh5-cre K^b cKO brains. f)
1057 Absolute counts of CD8 T cells in the brains of infected K^b Cre- Littermate and Cdh5-cre K^b
1058 cKO brains. g) Absolute counts of IFN-γ+ CD8 T cells in the brains of infected K^b Cre-
1059 Littermates and Cdh5-cre K^b cKOs. h) Absolute counts of IFN-γ+ CD4 T (Th1) cells in the
1060 brains of infected K^b Cre- Littermates and Cdh5-cre K^b cKOs. i) Absolute counts of CD11a+
1061 (antigen-experienced) CD8 T cells in the meninges, cLN and brain of infected K^b Cre-
1062 Littermates and Cdh5-cre K^b cKOs. Mice were injected with Alexa Fluor 488-anti-Thy1.2
1063 antibody ~3 min. before euthanasia. j) Quantified absolute counts of either IV+ or IV- antigen-
1064 experienced CD8 T cells in the brains of infected K^b Cre- Littermates and Cdh5-cre K^b cKOs. k)
1065 Frequency of IFN-γ+ CD8 T cells either labeled with IV antibody or negative for IV labeling. l)
1066 Representative UMAPs of D^b Cre- Littermate and Cdh5-cre D^b cKO brains, colorized with heat
1067 map of CD8 expression. m) Pie charts with corresponding frequencies of cell subset in D^b Cre-
1068 Littermate and Cdh5-cre D^b cKO brains (of CD45+) n) Absolute counts of CD4 T cells in the
1069 brains of infected D^b Cre- Littermate and Cdh5-cre D^b cKO brains. o) Absolute counts of CD8 T
1070 cells in the brains of infected D^b Cre- Littermate and Cdh5-cre D^b cKO brains. p) Absolute
1071 counts of IFN-γ+ CD8 T cells in the brains of infected D^b Cre- Littermates and Cdh5-cre D^b
1072 cKOs. q) Absolute counts of IFN-γ+ CD4 T (Th1) cells in the brains of infected D^b Cre-
1073 Littermates and Cdh5-cre D^b cKOs. r) Absolute counts of CD11a+ (antigen-experienced) CD8 T
1074 cells in the meninges, cLN and brain of infected D^b Cre- Littermates and Cdh5-cre D^b cKOs.
1075 Mice were injected with Alexa Fluor 488-anti-Thy1.2 antibody ~3 min. before euthanasia. s)
1076 Quantified absolute counts of either IV+ or IV- antigen-experienced CD8 T cells in the brains of
1077 infected D^b Cre- Littermates and Cdh5-cre D^b cKOs. t) Frequency of IFN-γ+ CD8 T cells either
1078 labeled with IV antibody or negative for IV labeling. Data were analyzed with unpaired t test or
1079 2way ANOVA with multiple comparisons. Scatterplots and bar plots present the mean ± SD. All
1080 p-values are shown or ns for non-significant p-value *($p > 0.05$)*.
1081
1082 **Fig 6. Vascular leakage during PbA infection is dependent on class I molecule expression**
1083 **on endothelium.** a) Top – Representative T1-weighted gadolinium enhanced MRI (sagittal slice)
1084 from K^b Cre- littermate day 6-8 PbA infection showing vascular leakage in regions of
1085 enhancement. Bottom - Representative T1-weighted gadolinium enhanced MRI (sagittal slice)
1086 from Cdh5-cre K^b cKO mice day 6-8 PbA infection with no vascular leakage or enhancement
1087 noted. Top right – 3D volumetric modeling of whole brain with vascular leakage highlighted in
1088 red. Top left – 3D volumetric modeling of whole brain with no apparent vascular leakage noted.
1089 b) Area measurements of regions of enhancement. Enhancement was quantified for each
1090 individual MRI slice and combined into a cumulative measurement per mouse. 2 blinded
1091 individuals performed measurements. Each data point represents the average of the scores for
1092 each mouse/scan. c) 3D pixelated volumetric measurement were obtained from all slices and
1093 averaged from 2 blinded reviewers as mentioned in b. d) FITC-albumin leakage assay results.
1094 Mice were IV injected with 66kDa FITC-conjugated albumin 1 hour prior to euthanasia to
1095 visualize regions of blood-brain barrier disruption and vascular leakage. e) Quantification of
1096 FITC-albumin mean fluorescence intensity per ROI. f) Top – Representative T1-weighted
1097 gadolinium enhanced MRI (sagittal slice) from D^b Cre- littermate day 6-8 PbA infection showing
1098 vascular leakage in regions of enhancement. Bottom - Representative T1-weighted gadolinium

1099 enhanced MRI (sagittal slice) from Cdh5-cre D^b cKO mice day 6-8 PbA infection with no
1100 vascular leakage or enhancement noted. Top right – 3D volumetric modeling of whole brain with
1101 vascular leakage highlighted in red. Top left – 3D volumetric modeling of whole brain with no
1102 apparent vascular leakage noted. g) Area measurements of regions of enhancement.
1103 Enhancement was quantified for each individual MRI slice and combined into a cumulative
1104 measurement per mouse. 2 blinded individuals performed measurements. Each data point
1105 represents the average of the scores for each mouse/scan. h) 3D pixelated volumetric
1106 measurement were obtained from all slices and averaged from 2 blinded reviewers as mentioned
1107 in g. i) FITC-albumin leakage assay results. Mice were IV injected with 66kDa FITC-conjugated
1108 albumin 1 hour prior to euthanasia to visualize regions of blood-brain barrier disruption and
1109 vascular leakage. j) Quantification of FITC-albumin mean fluorescence intensity per ROI. Data
1110 were analyzed with unpaired t test or 2way ANOVA with multiple comparisons. Violin plots and
1111 bar plots present the mean $\pm$ SD. All p-values are shown or ns for non-significant p-value *($p >$*
1112 *0.05)*.
1113
1114 **Fig 7. PbA infected parabionts sharing peripheral circulation demonstrate requirement of**
1115 **endothelial D^b expression for T cell responses and development of ECM.** a) Schematic
1116 depicting parabiosis procedure and respective D^b Cre- littermate and Cdh5-cre D^b cKO mice. b)
1117 Timeline of experiment depicting parabiosis surgery, healing and acclimation time and PbA
1118 infection of parabionts. c) Absolute counts of total CD45+ immune cells, CD8 T cells, CD4 T
1119 cells and activated CD8s and CD4s in the spleens of parabionts day 6 of PbA infection. d)
1120 Absolute counts of total CD45+ immune cells, CD8 T cells, CD4 T cells and activated CD8s and
1121 CD4s in the iLNs of parabionts day 6 of PbA infection. e) Absolute counts of total CD45+
1122 immune cells, CD8 T cells, CD4 T cells and IFN-γ producing CD8s and CD4s in the brains of
1123 parabionts day 6 of PbA infection. f) FITC-albumin was IV injected one hour before euthanasia
1124 of PbA infected parabionts. D^b Cre- littermate and Cdh5-cre D^b cKO parabiont brains are
1125 visualized with FITC leakage in green. g) T1-weighted gadolinium enhanced dual MRI of
1126 parabiont pair was performed. Representative image is one axial slice with visualization of
1127 gadolinium enhancement. Data were analyzed with unpaired t test. Bar plots present the mean $\pm$
1128 SD. All p-values are shown or ns for non-significant p-value *($p > 0.05$)*.
1129
1130 **Fig 8. Discrete class I molecules differentially regulate cell death and neuroinflammation in**
1131 **the brain during ECM.** Nanostring analysis was performed on whole brain isolated RNA of
1132 PbA infected C57BL/6, K^b and D^b Cre- littermates, Cdh5-cre K^b cKO, Cdh5-cre D^b cKO and
1133 uninfected controls of each group (n = 40, n = 4 mice/group). a) Venn diagrams of differentially
1134 expressed genes are visualized for comparison of differential class I regulation by wildtype mice,
1135 mice with only K^b and mice with only D^b expression. High-dimensional spectral flow cytometry
1136 was performed using a staining panel specific for stages of cell death. Frequencies of cells
1137 positive for markers of early apoptosis, late apoptosis and necrosis (late cell death) determined
1138 by annexin V staining vs viability stain gating. b) Frequencies of respective stages of cell death
1139 in Cre- littermates and Cdh5-cre K^b cKO expressed by brain endothelial cells on day 6 PbA
1140 infection. c) Frequencies of respective stages of cell death in Cre- littermates and Cdh5-cre K^b
1141 cKO expressed by mature neurons on day 6 PbA infection. d) Blinded clinical scoring was
1142 conducted daily on Cre- littermates and Cdh5-cre K^b cKO mice infected with PbA. e) Survival
1143 studies were performed on infected Cre- littermates and Cdh5-cre K^b cKO mice. Mice with K^b
1144 deletion had largely improved survival. f) Frequencies of respective stages of cell death in Cre-

1145 littermates and Cdh5-cre D^b cKO expressed by brain endothelial cells on day 6 PbA infection. g)
1146 Frequencies of respective stages of cell death in Cre- littermates and Cdh5-cre D^b cKO expressed
1147 by mature neurons on day 6 PbA infection. h) Blinded clinical scoring was conducted daily on
1148 Cre- littermates and Cdh5-cre D^b cKO mice infected with PbA. i) Survival studies were
1149 performed on infected Cre- littermates and Cdh5-cre D^b cKO mice. Mice with D^b deletion had
1150 vastly improved survival. j) IPA analysis was performed, and gene Expression Log Ration data
1151 was plotted in heat map to visualize changes in expression between groups. Data were analyzed
1152 with unpaired t test or 2way ANOVA with multiple comparisons. For survival, Kaplan Meier
1153 curves were plotted, and Log-rank (Mantel-Cox) curve comparison was performed. Scatter plots
1154 and bar plots present the mean $\pm$ SD. All p-values are shown or ns for non-significant p-value *(p*
1155 *> 0.05)*.
1156

1157 **Supplementary Table 1. IPA Causal network analysis identifies MHC Class I family as the**
1158 **number one master regulator of experimental cerebral malaria pathology.** Causal network
1159 analysis was performed using the Ingenuity Pathway Analysis application. Table includes
1160 normalized data from causal network analysis which identifies master regulators of the most
1161 highly enriched signaling pathways in the Nanostring dataset comparing uninfected C57BL/6
1162 brain vs. C57BL/6 brains with ECM. Master regulators of causal networks are listed in order of
1163 significance, with MHC Class I family identified as most significant causal network of
1164 experimental cerebral malaria pathology. P-value of overlap was adjusted using the Benjamini-
1165 Hochberg correction method.
1166
1167 **Supplementary Table 2. Differentially expressed genes in human endothelial cells after**
1168 ***Plasmodium* infection exposure.** Using GEO2R analysis platform MHC Class I was identified
1169 as one of the most significantly differentially expressed genes and was in the top 5 genes with
1170 significant upregulation on HBMECs after *Plasmodium* infection. Listed in order of significance.
1171
1172 **Supplementary Table 3. Patterns of neuroinflammation determined by cell specific gene**
1173 **enrichment during ECM determined through Mouse Glial Profiling Panel**. Table includes
1174 the nCounter Mouse Glial Profiling Panel gene lists, probes and corresponding cell type
1175 annotations detailing gene expression patterns and their corresponding neuroinflammatory
1176 response types.
1177
1178 **Supplementary Figure 1. Validation of human data comparison**. a) Boxplots show the
1179 distribution of the expression values for each human subject. Medians are centered indicating
1180 that human datasets are suitable for comparison. Value distribution analysis performed by
1181 GEO2R Web Application – NCBI GEO. b) MHC Class II Log_2 expression in control HBMECs
1182 vs. *Plasmodium* exposed HBMECs. Data were analyzed with unpaired t test (b). Box plots
1183 present the mean $\pm$ SD. All p-values are shown or ns for non-significant p-value *(p > 0.05)*.
1184
1185 **Supplementary Figure 2. Human and mouse antigen presentation pathways and**
1186 **corresponding genes show similar activation with *Plasmodium* infection.** Ingenuity Pathway
1187 analyses of mouse and human antigen presentation pathways are depicted in schematics.
1188 Coloring of the molecules corresponds to calculated z-scores (algorithm predicting activation or
1189 inhibition). Red indicates increased gene activation, orange indicates predicted activation of

pathways, green indicates decreased gene activation, blue indicates predicted inhibition of pathways, white indicates a z-score of zero with equal evidence for activation and inhibition, grey indicates that z-score could not be calculated.

Supplementary Figure 3. Peripheral immune system is intact K^b Cre- littermates and Cdh5-cre K^b cKO mice. a) Percentage of mTECs and cTECs quantified from thymi of naïve mice across groups and thymic weights of naïve mice across groups. b) Comparison of percentages of thymic T cell subsets in males vs females across groups in naïve mice. c) Percentages of respective VBeta TCRs out of CD8 T cells of the spleen in naïve mice. d) Splenic weights of naïve mice across groups. e) Absolute counts of CD45+ immune cells in respective peripheral organs of infected and naïve mice. f) Representative UMAPs depicting peripheral organs and immune cell populations and respective heats maps with CD44 activation marker expression. g) The scatter plots show quantified absolute cell counts of CD8 T cells, CD4 T cells and CD44hi CD8 T cells and CD4 T cells in the respective organs depicted in UMAPs. Data were analyzed with unpaired t test, Ordinary 1way ANOVA with multiple comparisons or 2way ANOVA with multiple comparisons. Scatterplots and bar plots present the mean $\pm$ SD. All p-values are shown or ns for non-significant p-value *($p > 0.05$)*.

Supplementary Figure 4. Peripheral immune system is intact in D^b Cre- littermates and Cdh5-cre D^b cKO mice. a) Percentage of mTECs and cTECs quantified from thymi of naïve mice across groups and thymic weights of naïve mice across groups. b) Comparison of percentages of thymic T cell subsets in males vs females across groups in naïve mice. c) Percentages of respective VBeta TCRs out of CD8 T cells of the spleen in naïve mice. d) Splenic weights of naïve mice across groups. e) Absolute counts of CD45+ immune cells in respective peripheral organs of infected mice. f) Scatter plots show quantified absolute cell counts of CD45+ immune cells, CD8 T cells, CD4 T cells and CD44hi CD8 T cells and CD4 T cells in respective organs of naïve mice. Data were analyzed with unpaired t test, Ordinary 1way ANOVA with multiple comparisons or 2way ANOVA with multiple comparisons. Scatterplots and bar plots present the mean $\pm$ SD. All p-values are shown or ns for non-significant p-value *($p > 0.05$)*.

Supplementary Figure 5. No changes to brain vasculature at baseline in mice with class I deletion on endothelium. a) Representative images from maximum intensity projections (MIPs) of naïve Cdh5-Cre K^b cKO and Cre- littermate controls. Mice were IP injected with gadolinium 15 min. before MRIs were performed. b) Quantification of 3D volume of overall brain vasculature enhancement and quantification of 3D pixelated voxel units. c) Representative images from maximum intensity projections (MIPs) of naïve Cdh5-Cre D^b cKO and Cre- littermate controls. Mice were IP injected with gadolinium 15 min. before MRIs were performed. d) Quantification of 3D volume of overall brain vasculature enhancement and quantification of 3D pixelated voxel units. Data were analyzed with unpaired t test. Scatterplots present the mean $\pm$ SD. All p-values are shown or ns for non-significant p-value *($p > 0.05$)*.

Supplementary Figure 6. CD8 T cells infiltrate regions of interest except when K^b is ablated from vasculature. a) Timeline depicting intracranial infection on Day 0 with TMEV or TMEV-OVA which is allowed to progress until day 7 when brains are harvested for high-dimensional spectral flow cytometry. b) Quantification of absolute counts of K^b: OVA_{257-}

1236 $_{264}^{+}$ CD8 T cells in Cdh5-Cre K^b cKO and Cre- littermate cLNs day 7 of TMEV-OVA infection.
1237 c) Quantification of absolute counts of D^b: $VP2^+$ CD8 T cells in Cdh5-Cre K^b cKO and Cre-
1238 littermate cLNs day 7 of TMEV infection. d) Absolute counts of CD45+ immune cells in the
1239 brains of Cdh5-Cre K^b cKO and Cre- littermate brains during ECM. e) Absolute counts of
1240 CD45+ immune cells in the brains of Cdh5-Cre D^b cKO and Cre- littermate brains during ECM.
1241 f) Quantified percentage of CD8s that are CXCR3+ in brains of Cdh5-Cre K^b cKO and Cre-
1242 littermates during ECM. g) Quantification of median fluorescence intensities of CXCR3 on CD8
1243 T cells in the brains of Cdh5-Cre K^b cKO and Cre- littermates during ECM. h) Quantified
1244 percentage of CD8s that are CCR7+ in brains during ECM. i) Quantification of median
1245 fluorescence intensities of CCR7 on CD8 T cells in the brain during ECM. j) Quantified
1246 percentage of CD8s that are CXCR3+ in brains of Cdh5-Cre D^b cKO and Cre- littermates during
1247 ECM. k) Quantification of median fluorescence intensities of CXCR3 on CD8 T cells in the
1248 brains of Cdh5-Cre D^b cKO and Cre- littermates during ECM. l) Quantified percentage of CD8s
1249 that are CCR7+ in brains during ECM. m) Quantification of median fluorescence intensities of
1250 CCR7 on CD8 T cells in the brain during ECM. n) Calculation of rate of infiltration of antigen-
1251 experienced CD11a+ CD8 T cells into the brain from IV labeled vasculature, measured in
1252 cells/min in infected K^b Cre- littermates and Cdh5-Cre K^b cKOs. o) Calculation of rate of
1253 infiltration of antigen-experienced CD11a+ CD8 T cells into the brain from IV labeled
1254 vasculature, measured in cells/min in infected D^b Cre- littermates and Cdh5-Cre D^b cKOs. p)
1255 Calculation of rate of infiltration of CD11a- CD8 T cells that have not encountered cognate
1256 peptide:MHC into the brain from IV labeled vasculature, measured in cells/min in infected K^b
1257 Cre- littermates and Cdh5-Cre K^b cKOs. q) Calculation of rate of infiltration of CD11a- CD8 T
1258 cells that have not encountered cognate peptide:MHC into the brain from IV labeled vasculature,
1259 measured in cells/min in infected D^b Cre- littermates and Cdh5-Cre D^b cKOs. Confocal imaging
1260 was performed. All images were acquired at 20X and zoomed in to 400X using FIJI. r)
1261 Representative immunofluorescence images of CD8 T cell infiltration in ROIs affected by ECM
1262 showing infiltration into these regions in the K^b Cre- littermates but not in the Cdh5-Cre K^b
1263 cKOs. Scale bar, 50 µM. s) Representative immunofluorescence images of CD8 T cell
1264 infiltration in ROIs affected by ECM showing infiltration into these regions in the D^b Cre-
1265 littermates and in the Cdh5-Cre D^b cKOs. Scale bar, 50 µM. Data were analyzed with unpaired t
1266 test. Bar plots present the mean $\pm$ SD. All p-values are shown or ns for non-significant p-value *(p*
1267 *> 0.05)*.
1268
1269 **Supplementary Figure 7. Tight junction protein alterations occur in human and mice with**
1270 **cerebral malaria.** GSEA was performed on HBMEC transcriptomic data. a) Enrichment plot
1271 showing a negative enrichment (downregulation) of molecular signature for tight junction gene
1272 set. The y-axis represents enrichment score (ES) and on the x-axis are genes (vertical black lines)
1273 represented in gene sets. The green line connects points of ES and genes. ES is the maximum
1274 deviation from zero as calculated for each gene going down the ranked list and represents the
1275 degree of over-representation of a gene set at the top or the bottom of the ranked gene list. The
1276 colored band at the bottom represents the degree of correlation of genes with the phenotype (red
1277 for positive and blue for negative correlation). Significance threshold set at nominal p-
1278 value < 0.05. Gene sets for tight junctions were significantly negatively enriched indicating
1279 downregulation in HBMECs during infection. Confocal imaging was performed. All images
1280 were acquired at 20X and zoomed in to 300X using FIJI. b) Immunofluorescence staining of
1281 tight junction protein Claudin-5 in ROI in PbA infected Cdh5-Cre K^b cKOs and K^b Cre-

littermates brains day 6. Scale bar, 50 µM. c) Immunofluorescence staining of tight junction protein Claudin-5 in ROI in PbA infected Cdh5-Cre D^b cKOs and D^b Cre- littermates day 6. Scale bar, 50 µM.

Supplementary Figure 8. Discrete endothelial class I molecules regulate differential downstream gene expression. a) Venn diagrams of differentially expressed genes are visualized for comparison of differential class I regulation in wildtype, K^b Cre- littermates and Cdh5-cre K^b cKO mice. Volcano plots of differentially expressed genes in whole brains of uninfected versus PbA infected groups of mice at endpoint during ECM. Significantly upregulated genes are indicated on upper right (purple dots). Significantly downregulated genes are indicated on upper left (turquoise dots). Horizontal dotted line indicates cutoff of adjusted p-values (-Log10 of adjusted p-value 1.3 corresponding to a threshold of p-value of 0.05). Vertical dotted line indicates cutoff of log2 Fold change (-1.5 to 1.5). b) Volcano plots of differentially expressed genes in infected K^b Cre- littermates vs Uninfected K^b Cre- littermates. c) Volcano plots of differentially expressed genes in infected Cdh5-cre K^b cKO mice vs Uninfected Cdh5-cre K^b cKO mice. d) Venn diagrams of differentially expressed genes are visualized for comparison of differential class I regulation in wildtype, D^b Cre- littermates and Cdh5-cre D^b cKO mice. e) Volcano plots of differentially expressed genes in infected D^b Cre- littermates vs Uninfected D^b Cre- littermates. f) Volcano plots of differentially expressed genes in infected Cdh5-cre D^b cKO mice vs Uninfected Cdh5-cre D^b cKO mice. P-values of overlap were adjusted using the Benjamini-Hochberg correction method.

References

1. Organization, W.H. World malaria report 2017. Geneva: WHO; 2017. 2018.

2. Organization, W.H. World malaria report 2021. (2021).

3. Idro, R., Marsh, K., John, C.C. & Newton, C.R. Cerebral malaria: mechanisms of brain injury and strategies for improved neurocognitive outcome. *Pediatr Res* **68**, 267-274 (2010).

4. Severe and complicated malaria. World Health Organization, Division of Control of Tropical Diseases. *Trans R Soc Trop Med Hyg* **84 Suppl 2**, 1-65 (1990).

5. Mahmoudi, S. & Keshavarz, H. Efficacy of phase 3 trial of RTS, S/AS01 malaria vaccine: The need for an alternative development plan. *Human vaccines & immunotherapeutics* **13**, 2098-2101 (2017).

6. Matuschewski, K. Vaccines against malaria—still a long way to go. *The FEBS journal* **284**, 2560-2568 (2017).

7. Rowe, A.K. *et al.* The burden of malaria mortality among African children in the year 2000. *Int J Epidemiol* **35**, 691-704 (2006).

8. Misra, U. *et al.* Cerebral malaria and bacterial meningitis. *Annals of Indian Academy of Neurology* **14**, S35 (2011).

9. Tunon-Ortiz, A. & Lamb, T.J. Blood brain barrier disruption in cerebral malaria: Beyond endothelial cell activation. *PLoS Pathogens* **15**, e1007786 (2019).

10. Seydel, K.B. *et al.* Brain swelling and death in children with cerebral malaria. *New England Journal of Medicine* **372**, 1126-1137 (2015).

11. Riggle, B.A. *et al.* CD8+ T cells target cerebrovasculature in children with cerebral malaria. *The Journal of clinical investigation* **130**, 1128-1138 (2020).

12. Ghazanfari, N., Mueller, S.N. & Heath, W.R. Cerebral malaria in mouse and man. *Frontiers in immunology* **9** (2018).

13. Finley, R., Mackey, L. & Lambert, P. Virulent P. berghei malaria: prolonged survival and decreased cerebral pathology in cell-dependent nude mice. *The Journal of Immunology* **129**, 2213-2218 (1982).

14. Yañez, D.M., Manning, D.D., Cooley, A.J., Weidanz, W.P. & Van Der Heyde, H. Participation of lymphocyte subpopulations in the pathogenesis of experimental murine cerebral malaria. *The Journal of Immunology* **157**, 1620-1624 (1996).

15. Nitcheu, J. *et al.* Perforin-dependent brain-infiltrating cytotoxic CD8+ T lymphocytes mediate experimental cerebral malaria pathogenesis. *The Journal of Immunology* **170**, 2221-2228 (2003).

16. Huggins, M.A. *et al.* Perforin expression by CD8 T cells is sufficient to cause fatal brain edema during experimental cerebral malaria. *Infection and immunity* **85**, e00985-00916 (2017).

17. Swanson, P.A. *et al.* CD8+ T cells induce fatal brainstem pathology during cerebral malaria via luminal antigen-specific engagement of brain vasculature. *PLoS pathogens* **12**, e1006022 (2016).

18. Takada, K. & Jameson, S.C. Self–class I MHC molecules support survival of naive CD8 T cells, but depress their functional sensitivity through regulation of CD8 expression levels. *Journal of Experimental Medicine* **206**, 2253-2269 (2009).

19. Tripathi, A.K., Sha, W., Shulaev, V., Stins, M.F. & Sullivan, D.J., Jr. Plasmodium falciparum-infected erythrocytes induce NF-kappaB regulated inflammatory pathways in human cerebral endothelium. *Blood* **114**, 4243-4252 (2009).

1371 20. Combes, V. *et al.* Pathogenic role of P-selectin in experimental cerebral malaria:
1372 importance of the endothelial compartment. *The American journal of pathology* **164**, 781-
1373 786 (2004).
1374
1375 21. Goddery, E.N. *et al.* Microglia and perivascular macrophages act as antigen presenting
1376 cells to promote CD8 T cell infiltration of the brain. *Frontiers in immunology*, 3428
1377 (2021).
1378
1379 22. Suidan, G.L., Mcdole, J.R., Chen, Y., Pirko, I. & Johnson, A.J. Induction of blood brain
1380 barrier tight junction protein alterations by CD8 T cells. *PloS one* **3**, e3037 (2008).
1381
1382 23. Pavelko, K.D. *et al.* Theiler's murine encephalomyelitis virus as a vaccine candidate for
1383 immunotherapy. *PloS one* **6**, e20217 (2011).
1384
1385 24. Campanella, G.S. *et al.* Chemokine receptor CXCR3 and its ligands CXCL9 and
1386 CXCL10 are required for the development of murine cerebral malaria. *Proceedings of the*
1387 *National Academy of Sciences* **105**, 4814-4819 (2008).
1388
1389 25. Ghazanfari, N., Mueller, S.N. & Heath, W.R. Cerebral malaria in mouse and man.
1390 *Frontiers in immunology*, 2016 (2018).
1391
1392 26. Cupovic, J. *et al.* Central nervous system stromal cells control local CD8+ T cell
1393 responses during virus-induced neuroinflammation. *Immunity* **44**, 622-633 (2016).
1394
1395 27. Zhao, H. *et al.* Olfactory plays a key role in spatiotemporal pathogenesis of cerebral
1396 malaria. *Cell host & microbe* **15**, 551-563 (2014).
1397
1398 28. Rai, D., Pham, N.-L.L., Harty, J.T. & Badovinac, V.P. Tracking the total CD8 T cell
1399 response to infection reveals substantial discordance in magnitude and kinetics between
1400 inbred and outbred hosts. *The Journal of Immunology* **183**, 7672-7681 (2009).
1401
1402 29. Bhat, P., Leggatt, G., Waterhouse, N. & Frazer, I.H. Interferon-γ derived from cytotoxic
1403 lymphocytes directly enhances their motility and cytotoxicity. *Cell death & disease* **8**,
1404 e2836-e2836 (2017).
1405
1406 30. Krasemann, S. *et al.* The TREM2-APOE pathway drives the transcriptional phenotype of
1407 dysfunctional microglia in neurodegenerative diseases. *Immunity* **47**, 566-581. e569
1408 (2017).
1409
1410 31. Keren-Shaul, H. *et al.* A unique microglia type associated with restricting development of
1411 Alzheimer's disease. *Cell* **169**, 1276-1290. e1217 (2017).
1412
1413 32. Aguzzi, A., Barres, B.A. & Bennett, M.L. Microglia: scapegoat, saboteur, or something
1414 else? *Science* **339**, 156-161 (2013).
1415

1416 33. Deczkowska, A. *et al.* Disease-associated microglia: a universal immune sensor of
1417 neurodegeneration. *Cell* **173**, 1073-1081 (2018).
1418
1419 34. Pais, T.F. & Penha-Gonçalves, C. Brain endothelium: the "innate immunity response
1420 hypothesis" in cerebral malaria pathogenesis. *Frontiers in immunology* **9**, 3100 (2019).
1421
1422 35. Carman, C.V. & Martinelli, R. T lymphocyte–endothelial interactions: emerging
1423 understanding of trafficking and antigen-specific immunity. *Frontiers in immunology* **6**,
1424 603 (2015).
1425
1426 36. Waisman, A. & Johann, L. Antigen-presenting cell diversity for T cell reactivation in
1427 central nervous system autoimmunity. *Journal of Molecular Medicine* **96**, 1279-1292
1428 (2018).
1429
1430 37. Amersfoort, J., Eelen, G. & Carmeliet, P. Immunomodulation by endothelial cells—
1431 partnering up with the immune system? *Nature Reviews Immunology*, 1-13 (2022).
1432
1433 38. Murphy, K. & Weaver, C. *Janeway's immunobiology*. Garland science, 2016.
1434
1435 39. Engelhardt, B. & Ransohoff, R.M. The ins and outs of T-lymphocyte trafficking to the
1436 CNS: anatomical sites and molecular mechanisms. *Trends in immunology* **26**, 485-495
1437 (2005).
1438
1439 40. Laschinger, M. & Engelhardt, B. Interaction of α4-integrin with VCAM-1 is involved in
1440 adhesion of encephalitogenic T cell blasts to brain endothelium but not in their
1441 transendothelial migration in vitro. *Journal of neuroimmunology* **102**, 32-43 (2000).
1442
1443 41. Marchetti, L. & Engelhardt, B. Immune cell trafficking across the blood-brain barrier in
1444 the absence and presence of neuroinflammation. *Vascular Biology* **2**, H1-H18 (2020).
1445
1446 42. Sathiyanadan, K., Coisne, C., Enzmann, G., Deutsch, U. & Engelhardt, B. PSGL-1 and
1447 E/P-selectins are essential for T-cell rolling in inflamed CNS microvessels but
1448 dispensable for initiation of EAE. *European journal of immunology* **44**, 2287-2294
1449 (2014).
1450
1451 43. Villegas-Mendez, A. *et al.* IFN-γ–producing CD4+ T cells promote experimental cerebral
1452 malaria by modulating CD8+ T cell accumulation within the brain. *The Journal of*
1453 *Immunology* **189**, 968-979 (2012).
1454
1455 44. Krausgruber, T. *et al.* Structural cells are key regulators of organ-specific immune
1456 responses. *Nature* **583**, 296-302 (2020).
1457
1458 45. Howland, S.W. *et al.* Brain microvessel cross-presentation is a hallmark of experimental
1459 cerebral malaria. *EMBO molecular medicine* **5**, 984-999 (2013).
1460

1461 46. Belnoue, E. *et al.* Control of pathogenic CD8+ T cell migration to the brain by IFN-γ
1462 during experimental cerebral malaria. *Parasite immunology* **30**, 544-553 (2008).
1463
1464 47. Suidan, G.L. *et al.* CD8 T cell-initiated vascular endothelial growth factor expression
1465 promotes central nervous system vascular permeability under neuroinflammatory
1466 conditions. *The journal of immunology* **184**, 1031-1040 (2010).
1467
1468 48. Miyakoda, M. *et al.* Malaria-specific and nonspecific activation of CD8+ T cells during
1469 blood stage of Plasmodium berghei infection. *The Journal of Immunology* **181**, 1420-
1470 1428 (2008).
1471
1472 49. Poh, C.M., Howland, S.W., Grotenbreg, G.M. & Rénia, L. Damage to the blood-brain
1473 barrier during experimental cerebral malaria results from synergistic effects of CD8+ T
1474 cells with different specificities. *Infection and immunity* **82**, 4854-4864 (2014).
1475
1476 50. Kalkal, M. *et al.* A comprehensive study of epitopes and immune reactivity among
1477 Plasmodium species. *BMC microbiology* **22**, 1-14 (2022).
1478
1479 51. Pardy, R.D. *et al.* Analysis of the T cell response to Zika virus and identification of a
1480 novel CD8+ T cell epitope in immunocompetent mice. *PLoS pathogens* **13**, e1006184
1481 (2017).
1482
1483 52. Mora, J.R. & von Andrian, U.H. T-cell homing specificity and plasticity: new concepts
1484 and future challenges. *Trends in immunology* **27**, 235-243 (2006).
1485
1486 53. Ioannidis, L.J., Nie, C.Q. & Hansen, D.S. The role of chemokines in severe malaria: more
1487 than meets the eye. *Parasitology* **141**, 602-613 (2014).
1488
1489 54. Miu, J. *et al.* Chemokine gene expression during fatal murine cerebral malaria and
1490 protection due to CXCR3 deficiency. *The Journal of Immunology* **180**, 1217-1230
1491 (2008).
1492
1493 55. Strangward, P. *et al.* A quantitative brain map of experimental cerebral malaria
1494 pathology. *PLoS pathogens* **13**, e1006267 (2017).
1495
1496 56. Solouki, S. *et al.* TCR signal strength and antigen affinity regulate CD8+ memory T
1497 cells. *The Journal of Immunology* **205**, 1217-1227 (2020).
1498
1499 57. Tan, M. *et al.* T cell receptor binding affinity governs the functional profile of cancer-
1500 specific CD8+ T cells. *Clinical & Experimental Immunology* **180**, 255-270 (2015).
1501
1502 58. Irving, M. *et al.* Interplay between T cell receptor binding kinetics and the level of
1503 cognate peptide presented by major histocompatibility complexes governs CD8+ T cell
1504 responsiveness. *Journal of Biological Chemistry* **287**, 23068-23078 (2012).
1505

1506 59. Martinez, R.J. & Evavold, B.D. Lower affinity T cells are critical components and active
1507 participants of the immune response. *Frontiers in immunology* **6**, 468 (2015).
1508
1509 60. Tau, G.Z., Cowan, S.N., Weisburg, J., Braunstein, N.S. & Rothman, P.B. Regulation of
1510 IFN-γ signaling is essential for the cytotoxic activity of CD8+ T cells. *The Journal of*
1511 *Immunology* **167**, 5574-5582 (2001).
1512
1513 61. Malo, C.S. *et al.* Non-equivalent antigen presenting capabilities of dendritic cells and
1514 macrophages in generating brain-infiltrating CD8+ T cell responses. *Nature*
1515 *communications* **9**, 1-13 (2018).
1516
1517 62. Tritz, Z.P. *et al.* Conditional Silencing of H-2Db Class I Molecule Expression Modulates
1518 the Protective and Pathogenic Kinetics of Virus-Antigen–Specific CD8 T Cell Responses
1519 during Theiler's Virus Infection. *The Journal of Immunology* **205**, 1228-1238 (2020).
1520
1521 63. Hortle, E. *et al.* KCC1 Activation protects Mice from the Development of Experimental
1522 Cerebral Malaria. *Scientific reports* **9**, 1-11 (2019).
1523
1524 64. Organization, W.H. & Control, C.f.D. *Basic malaria microscopy: tutor's guide*. World
1525 Health Organization, 2010.
1526
1527 65. Johnson, H.L. *et al.* CD8 T cell-initiated blood–brain barrier disruption is independent of
1528 neutrophil support. *The Journal of Immunology* **189**, 1937-1945 (2012).
1529
1530 66. Garcia, L.M.C., Kelcher, A.M.H., Malo, C.S. & Johnson, A.J. Superior isolation of
1531 antigen-specific brain infiltrating T cells using manual homogenization technique.
1532 *Journal of immunological methods* **439**, 23-28 (2016).
1533
1534 67. Rustenhoven, J. *et al.* Functional characterization of the dural sinuses as a neuroimmune
1535 interface. *Cell* **184**, 1000-1016. e1027 (2021).
1536
1537 68. Liu, Y.U. *et al.* Neuronal network activity controls microglial process surveillance in
1538 awake mice via norepinephrine signaling. *Nature neuroscience* **22**, 1771-1781 (2019).
1539
1540 69. Eyo, U.B. *et al.* P2Y12R-Dependent Translocation Mechanisms Gate the Changing
1541 Microglial Landscape. *Cell reports* **23**, 959-966 (2018).
1542
1543 70. Schindelin, J. *et al.* Fiji: an open-source platform for biological-image analysis. *Nature*
1544 *methods* **9**, 676-682 (2012).
1545
1546 71. Shakhar, G. *et al.* Stable T cell-dendritic cell interactions precede the development of
1547 both tolerance and immunity in vivo. *Nature immunology* **6**, 707-714 (2005).
1548
1549 72. Tripathi, A.K., Sullivan, D.J. & Stins, M.F. Plasmodium falciparum-infected erythrocytes
1550 increase intercellular adhesion molecule 1 expression on brain endothelium through NF-
1551 κB. *Infection and immunity* **74**, 3262-3270 (2006).

73. Barrett, T. *et al.* NCBI GEO: archive for functional genomics data sets—update. *Nucleic acids research* **41**, D991-D995 (2012).

74. Subramanian, A. *et al.* Gene set enrichment analysis: a knowledge-based approach for interpreting genome-wide expression profiles. *Proceedings of the National Academy of Sciences* **102**, 15545-15550 (2005).

Figure 1

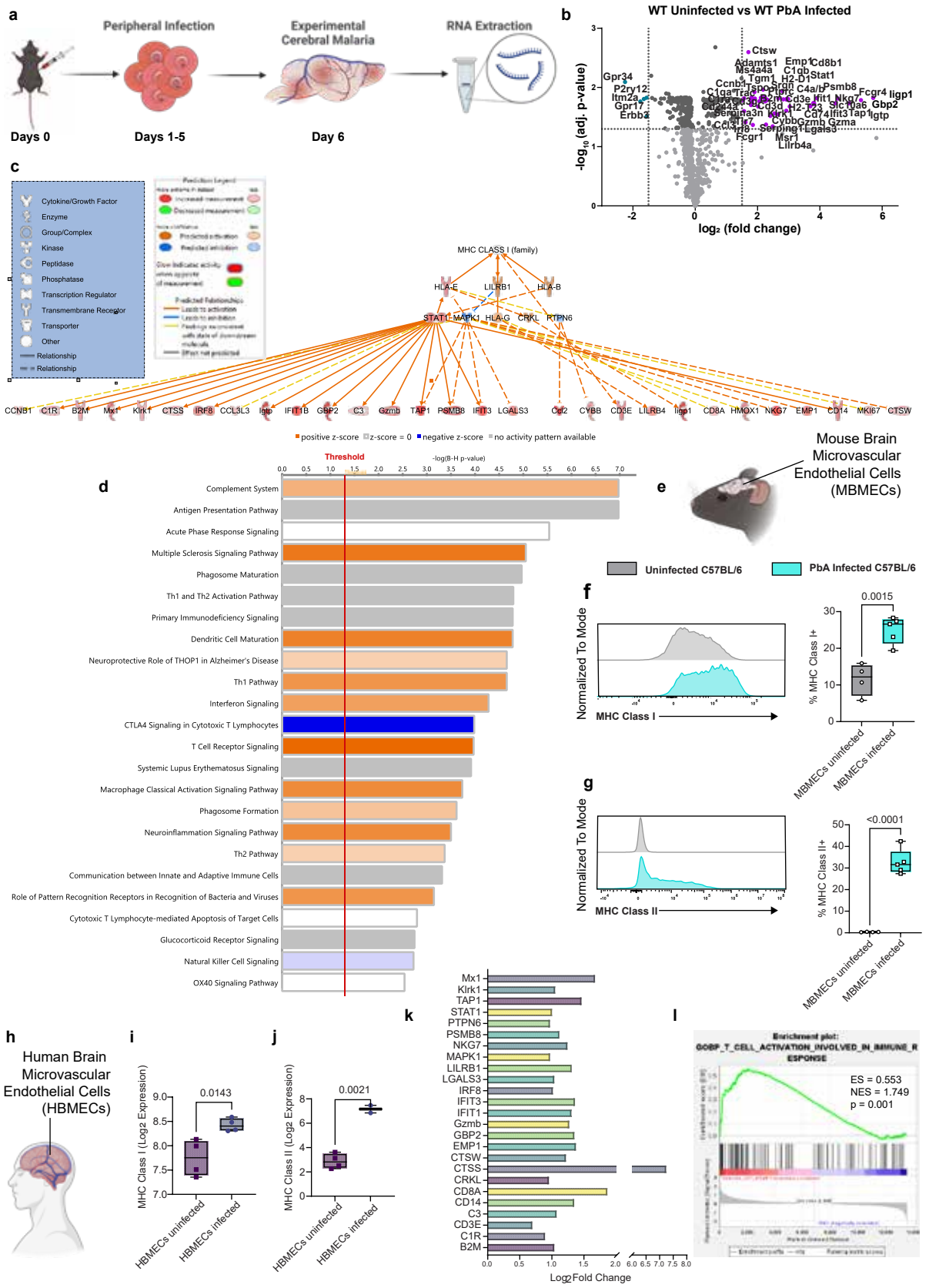
a
Peripheral Infection
Experimental Cerebral Malaria
RNA Extraction
Days 0
Days 1-5
Day 6
b
WT Uninfected vs WT PbA Infected
-log10 (adj. p-value)
log2 (fold change)
c
Cytokine/Growth Factor
Enzyme
Group/Complex
Kinase
Peptidase
Phosphatase
Transcription Regulator
Transmembrane Receptor
Transporter
Other
Relationship
Relationship
MHC CLASS I (family)
HLA-E
LILRB1
HLA-B
STAT1
MAPK1
HLA-G
CRKL
RTPN6
CCNB1 C1R B2M Mx1 Klrk1 CTSS IRF8 CCL3L3 Igtp IFIT1B GBP2 C3 Gzmb TAP1 PSMB8 IFIT3 LGALS3 Ccl2 CYBB CD3E LILRB4 Iigp1 CD8A HMOX1 NKG7 EMP1 CD14 MKI67 CTSW
positive z-score
z-score = 0
negative z-score
no activity pattern available
d
Threshold
-log(B-H p-value)
Complement System
Antigen Presentation Pathway
Acute Phase Response Signaling
Multiple Sclerosis Signaling Pathway
Phagosome Maturation
Th1 and Th2 Activation Pathway
Primary Immunodeficiency Signaling
Dendritic Cell Maturation
Neuroprotective Role of THOP1 in Alzheimer's Disease
Th1 Pathway
Interferon Signaling
CTLA4 Signaling in Cytotoxic T Lymphocytes
T Cell Receptor Signaling
Systemic Lupus Erythematosus Signaling
Macrophage Classical Activation Signaling Pathway
Phagosome Formation
Neuroinflammation Signaling Pathway
Th2 Pathway
Communication between Innate and Adaptive Immune Cells
Role of Pattern Recognition Receptors in Recognition of Bacteria and Viruses
Cytotoxic T Lymphocyte-mediated Apoptosis of Target Cells
Glucocorticoid Receptor Signaling
Natural Killer Cell Signaling
OX40 Signaling Pathway
e
Mouse Brain Microvascular Endothelial Cells (MBMECs)
Uninfected C57BL/6
PbA Infected C57BL/6
f
Normalized To Mode
MHC Class I
% MHC Class I+
0.0015
MBMECs uninfected
MBMECs infected
g
Normalized To Mode
MHC Class II
% MHC Class II+
<0.0001
MBMECs uninfected
MBMECs infected
h
Human Brain Microvascular Endothelial Cells (HBMECs)
i
MHC Class I (Log2 Expression)
0.0143
HBMECs uninfected
HBMECs infected
j
MHC Class II (Log2 Expression)
0.0021
HBMECs uninfected
HBMECs infected
k
Mx1
Klrk1
TAP1
STAT1
PTPN6
PSMB8
NKG7
MAPK1
LILRB1
LGALS3
IRF8
IFIT3
IFIT1
Gzmb
GBP2
EMP1
CTSW
CTSS
CRKL
CD8A
CD14
C3
CD3E
C1R
B2M
Log2 Fold Change
l
Enrichment plot:
GOBP_T_CELL_ACTIVATION_INVOLVED_IN_IMMUNE_RESPONSE
ES = 0.553
NES = 1.749
p = 0.001

Figure 2

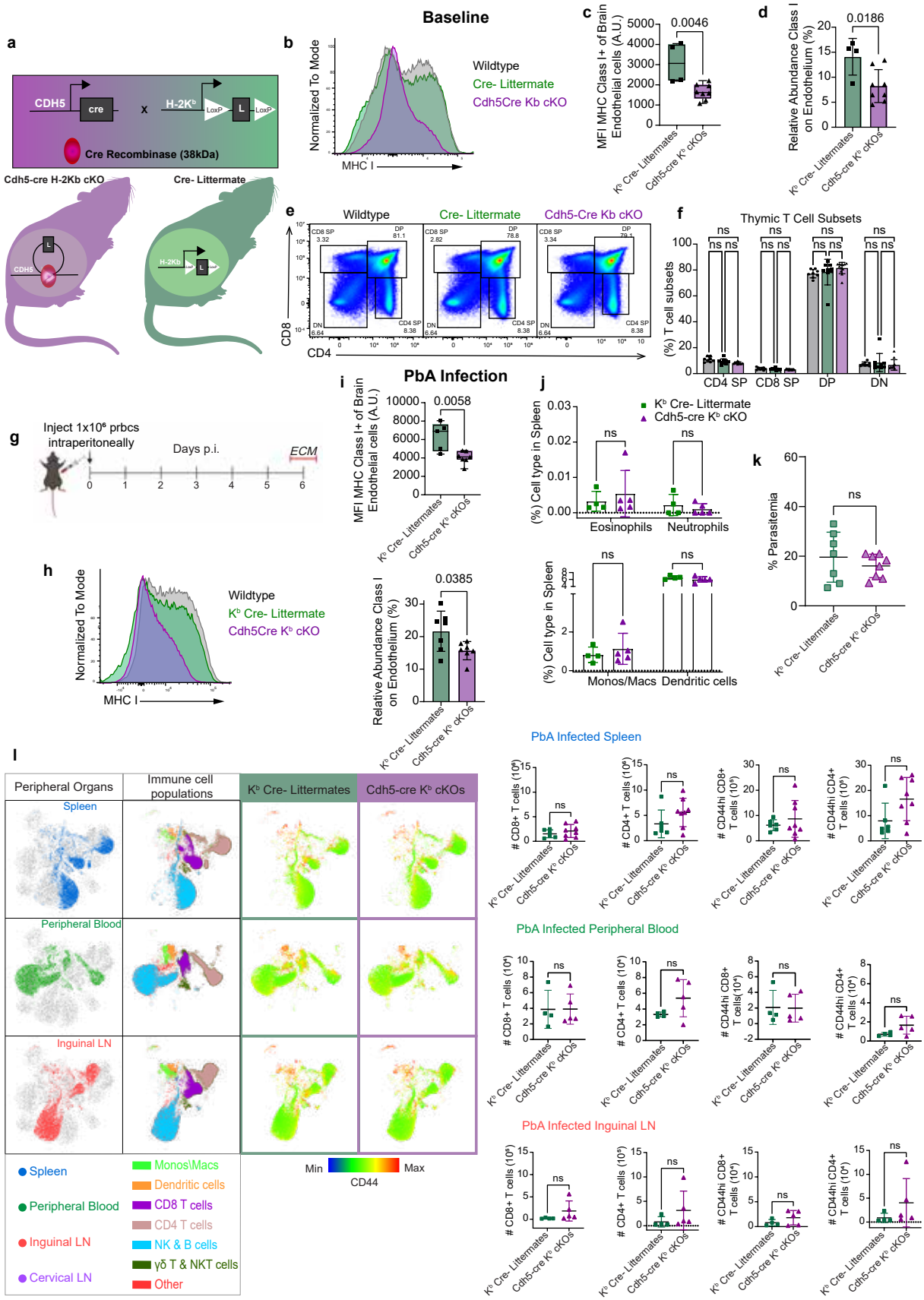
a
CDH5
cre
x
H-2Kᵇ
LoxP
L
LoxP
Cre Recombinase (38kDa)
Cdh5-cre H-2Kb cKO
Cre- Littermate
b
Baseline
Normalized To Mode
MHC I
Wildtype
Cre- Littermate
Cdh5Cre Kb cKO
c
MFI MHC Class I+ of Brain Endothelial cells (A.U.)
0.0046
Kᵇ Cre- Littermates
Cdh5-cre Kᵇ cKOs
d
Relative Abundance Class I on Endothelium (%)
0.0186
e
Wildtype
Cre- Littermate
Cdh5-Cre Kb cKO
CD8
CD4
f
Thymic T Cell Subsets
(%) T cell subsets
ns
CD4 SP
CD8 SP
DP
DN
g
Inject 1x10⁶ prbcs intraperitoneally
Days p.i.
ECM
0
1
2
3
4
5
6
h
Normalized To Mode
MHC I
Wildtype
Kᵇ Cre- Littermate
Cdh5Cre Kᵇ cKO
i
PbA Infection
MFI MHC Class I+ of Brain Endothelial cells (A.U.)
0.0058
Relative Abundance Class I on Endothelium (%)
0.0385
j
Kᵇ Cre- Littermate
Cdh5-cre Kᵇ cKO
(%) Cell type in Spleen
Eosinophils
Neutrophils
Monos/Macs
Dendritic cells
k
% Parasitemia
l
Peripheral Organs
Immune cell populations
Kᵇ Cre- Littermates
Cdh5-cre Kᵇ cKOs
Spleen
Peripheral Blood
Inguinal LN
Min
Max
CD44
Spleen
Peripheral Blood
Inguinal LN
Cervical LN
Monos\Macs
Dendritic cells
CD8 T cells
CD4 T cells
NK & B cells
γδ T & NKT cells
Other
PbA Infected Spleen
CD8+ T cells (10⁶)
CD4+ T cells (10⁶)
CD44hi CD8+ T cells (10⁶)
CD44hi CD4+ T cells (10⁶)
PbA Infected Peripheral Blood
PbA Infected Inguinal LN

Figure 3

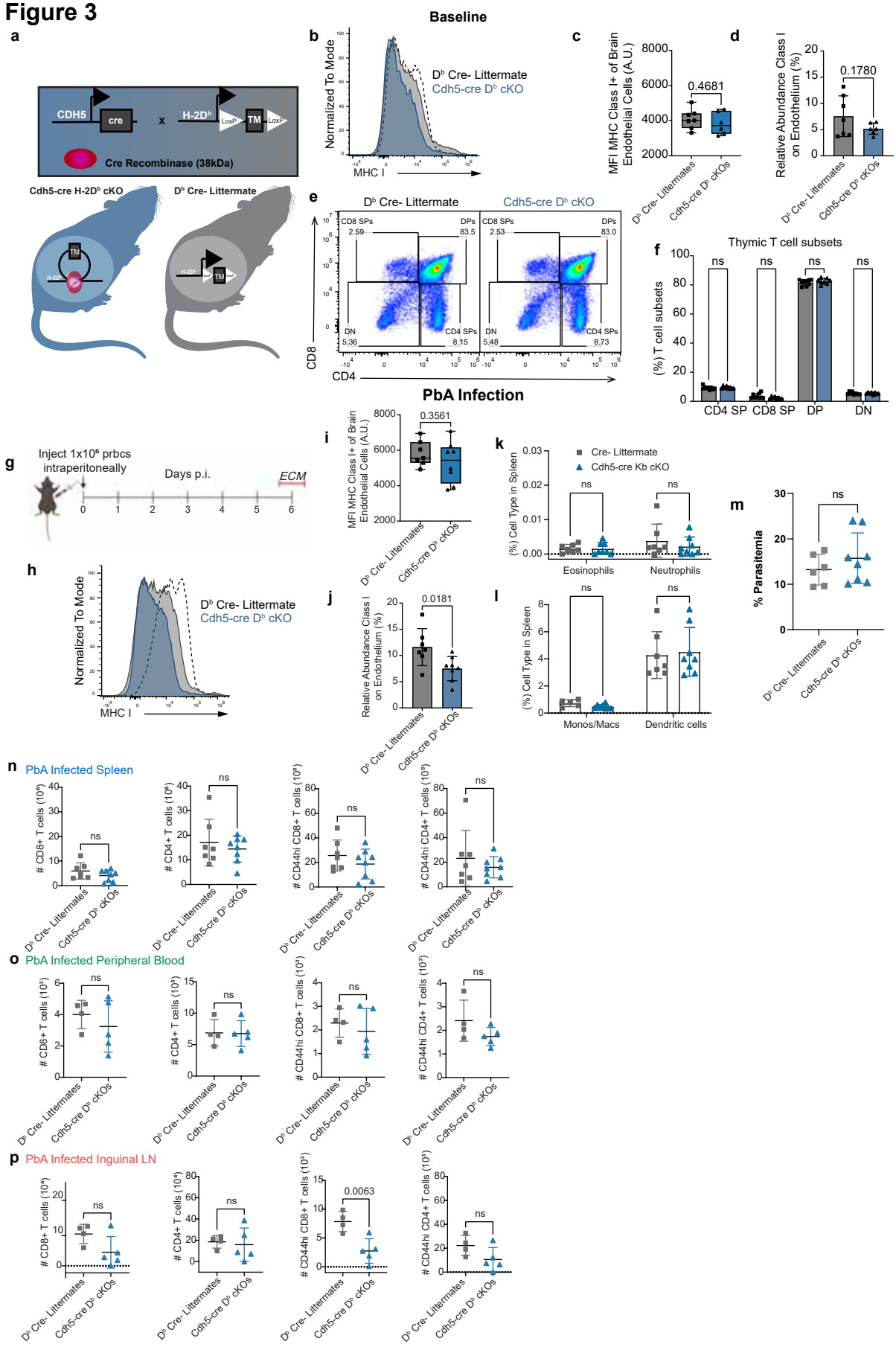
a
CDH5
cre
x
H-2Dᵇ
LoxP
TM
LoxP
Cre Recombinase (38kDa)
Cdh5-cre H-2Dᵇ cKO
Dᵇ Cre- Littermate
Baseline
b
Normalized To Mode
Dᵇ Cre- Littermate
Cdh5-cre Dᵇ cKO
MHC I
c
MFI MHC Class I+ of Brain Endothelial Cells (A.U.)
0.4681
Dᵇ Cre- Littermates
Cdh5-cre Dᵇ cKOs
d
Relative Abundance Class I on Endothelium (%)
0.1780
e
Dᵇ Cre- Littermate
Cdh5-cre Dᵇ cKO
CD8 SPs
DPs
DN
CD4 SPs
CD8
CD4
f
Thymic T cell subsets
(%) T cell subsets
ns
CD4 SP
CD8 SP
DP
DN
PbA Infection
g
Inject 1x10⁶ prbcs intraperitoneally
Days p.i.
ECM
h
Normalized To Mode
Dᵇ Cre- Littermate
Cdh5-cre Dᵇ cKO
MHC I
i
MFI MHC Class I+ of Brain Endothelial Cells (A.U.)
0.3561
j
Relative Abundance Class I on Endothelium (%)
0.0181
k
Cre- Littermate
Cdh5-cre Kb cKO
(%) Cell Type in Spleen
Eosinophils
Neutrophils
l
Monos/Macs
Dendritic cells
m
% Parasitemia
n
PbA Infected Spleen
CD8+ T cells (10⁴)
CD4+ T cells (10⁴)
CD44hi CD8+ T cells (10⁴)
CD44hi CD4+ T cells (10⁴)
o
PbA Infected Peripheral Blood
CD8+ T cells (10³)
CD4+ T cells (10³)
CD44hi CD8+ T cells (10³)
CD44hi CD4+ T cells (10³)
p
PbA Infected Inguinal LN
CD8+ T cells (10⁴)
CD4+ T cells (10⁴)
CD44hi CD8+ T cells (10³)
0.0063
CD44hi CD4+ T cells (10³)

Figure 4

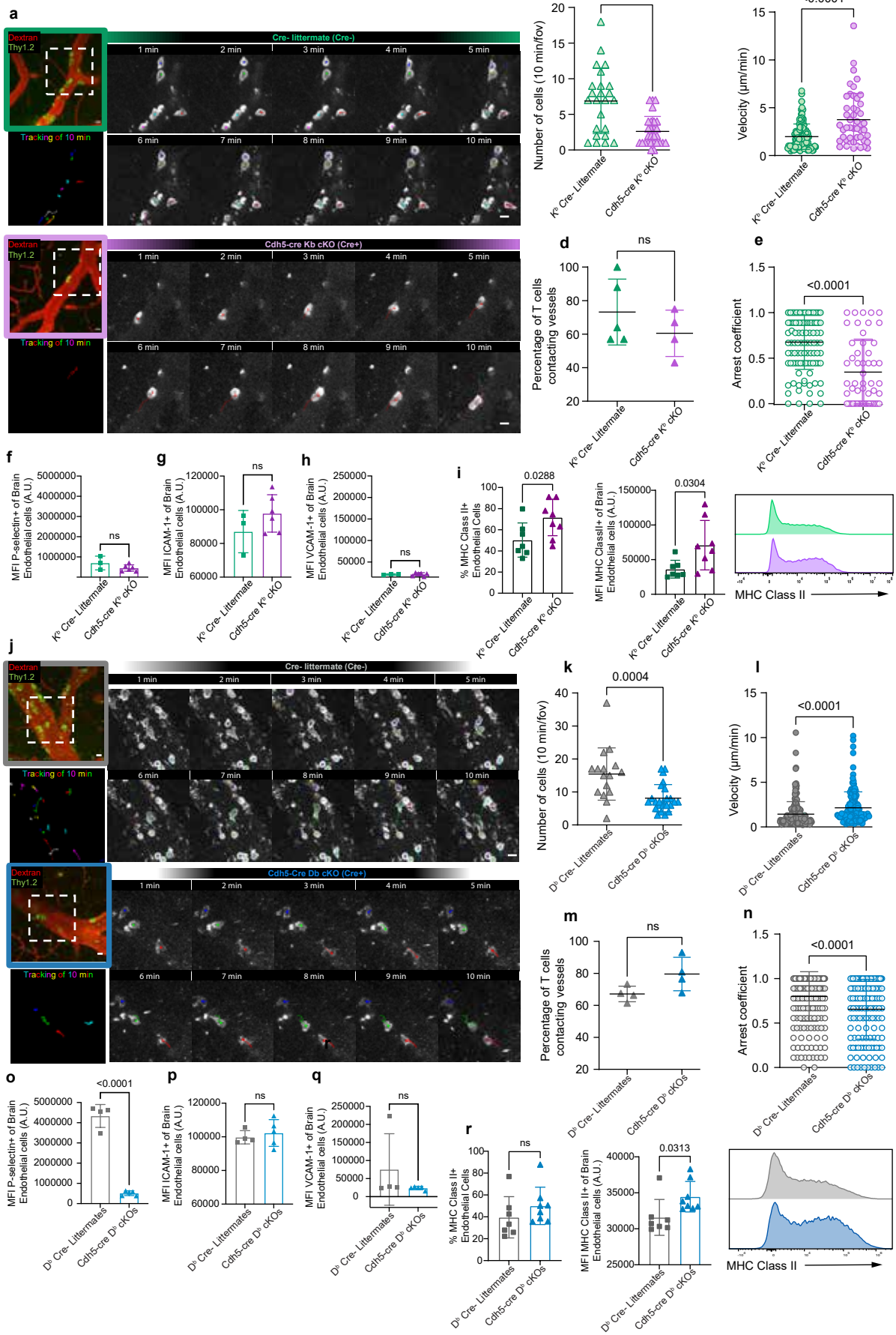
a
Dextran
Thy1.2
Cre- littermate (Cre-)
1 min
2 min
3 min
4 min
5 min
Tracking of 10 min
6 min
7 min
8 min
9 min
10 min
Cdh5-cre Kb cKO (Cre+)
b
0.0002
Number of cells (10 min/fov)
Kᵇ Cre- Littermate
Cdh5-cre Kᵇ cKO
c
<0.0001
Velocity (µm/min)
d
ns
Percentage of T cells contacting vessels
e
<0.0001
Arrest coefficient
f
MFI P-selectin+ of Brain Endothelial cells (A.U.)
g
MFI ICAM-1+ of Brain Endothelial cells (A.U.)
h
MFI VCAM-1+ of Brain Endothelial cells (A.U.)
i
0.0288
% MHC Class II+ Endothelial Cells
0.0304
MFI MHC ClassII+ of Brain Endothelial cells (A.U.)
MHC Class II
j
Cre- littermate (Cre-)
Cdh5-Cre Db cKO (Cre+)
k
0.0004
Dᵇ Cre- Littermates
Cdh5-cre Dᵇ cKOs
l
<0.0001
m
ns
Percentage of T cells contacting vessels
n
<0.0001
Arrest coefficient
o
<0.0001
p
ns
q
ns
r
ns
% MHC Class II+ Endothelial Cells
0.0313
MFI MHC Class II+ of Brain Endothelial cells (A.U.)
MHC Class II

Figure 5

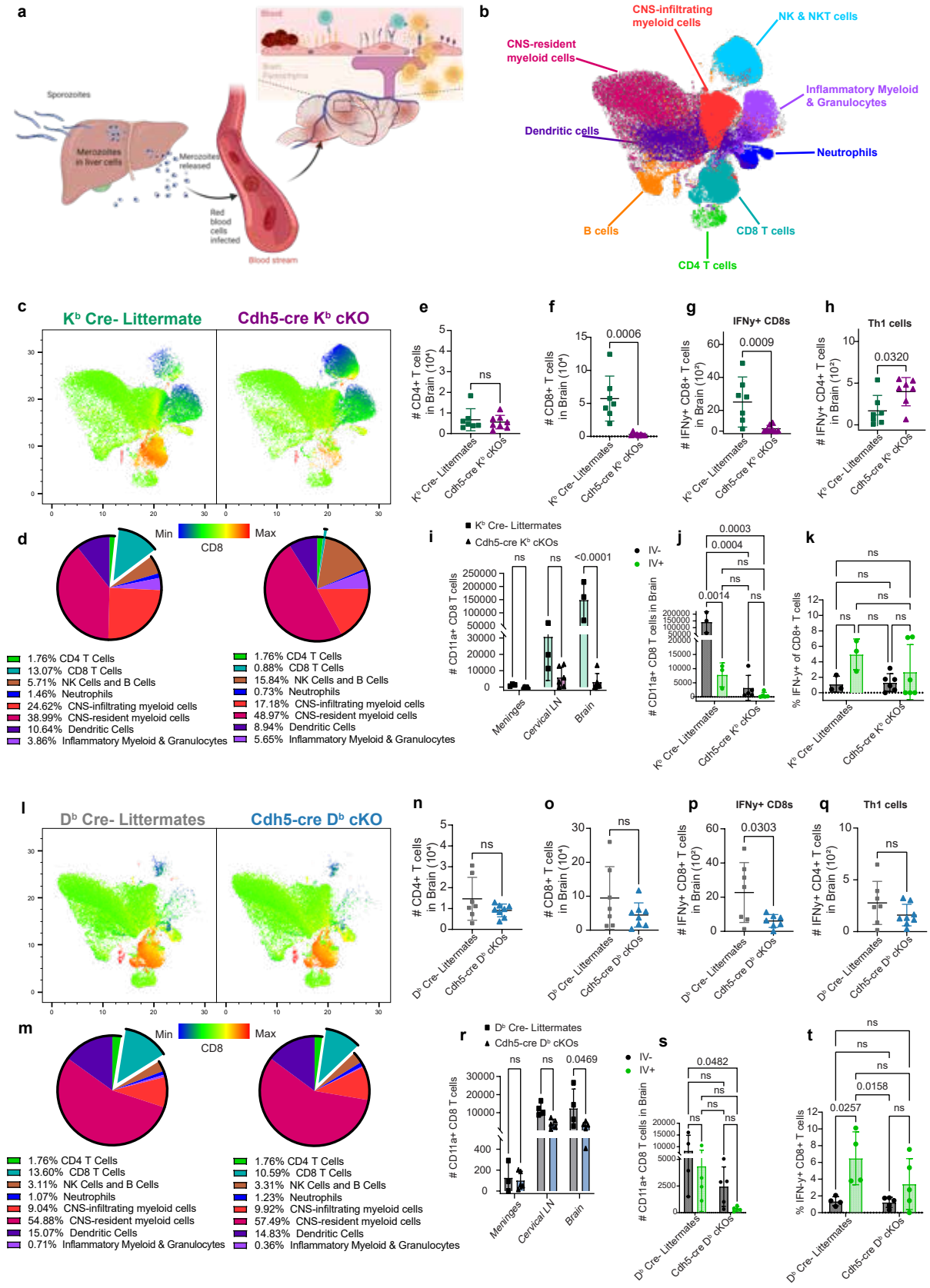
a
Sporozoites
Merozoites in liver cells
Merozoites released
Red blood cells infected
Blood stream
b
CNS-infiltrating myeloid cells
NK & NKT cells
CNS-resident myeloid cells
Inflammatory Myeloid & Granulocytes
Dendritic cells
Neutrophils
B cells
CD8 T cells
CD4 T cells
c
Kᵇ Cre- Littermate
Cdh5-cre Kᵇ cKO
d
Min
CD8
Max
1.76% CD4 T Cells
13.07% CD8 T Cells
5.71% NK Cells and B Cells
1.46% Neutrophils
24.62% CNS-infiltrating myeloid cells
38.99% CNS-resident myeloid cells
10.64% Dendritic Cells
3.86% Inflammatory Myeloid & Granulocytes
1.76% CD4 T Cells
0.88% CD8 T Cells
15.84% NK Cells and B Cells
0.73% Neutrophils
17.18% CNS-infiltrating myeloid cells
48.97% CNS-resident myeloid cells
8.94% Dendritic Cells
5.65% Inflammatory Myeloid & Granulocytes
e
CD4+ T cells in Brain (10⁴)
ns
Kᵇ Cre- Littermates
Cdh5-cre Kᵇ cKOs
f
CD8+ T cells in Brain (10⁴)
0.0006
g
IFNγ+ CD8s
IFNγ+ CD8+ T cells in Brain (10³)
0.0009
h
Th1 cells
IFNγ+ CD4+ T cells in Brain (10³)
0.0320
i
Kᵇ Cre- Littermates
Cdh5-cre Kᵇ cKOs
CD11a+ CD8 T cells
ns
ns
<0.0001
Meninges
Cervical LN
Brain
j
IV-
IV+
CD11a+ CD8 T cells in Brain
0.0003
0.0004
ns
0.0014
ns
k
% IFNγ+ of CD8+ T cells
ns
ns
ns
ns
l
Dᵇ Cre- Littermates
Cdh5-cre Dᵇ cKO
m
Min
CD8
Max
1.76% CD4 T Cells
13.60% CD8 T Cells
3.11% NK Cells and B Cells
1.07% Neutrophils
9.04% CNS-infiltrating myeloid cells
54.88% CNS-resident myeloid cells
15.07% Dendritic Cells
0.71% Inflammatory Myeloid & Granulocytes
1.76% CD4 T Cells
10.59% CD8 T Cells
3.31% NK Cells and B Cells
1.23% Neutrophils
9.92% CNS-infiltrating myeloid cells
57.49% CNS-resident myeloid cells
14.83% Dendritic Cells
0.36% Inflammatory Myeloid & Granulocytes
n
CD4+ T cells in Brain (10⁴)
ns
Dᵇ Cre- Littermates
Cdh5-cre Dᵇ cKOs
o
CD8+ T cells in Brain (10⁴)
ns
p
IFNγ+ CD8s
IFNγ+ CD8+ T cells in Brain (10³)
0.0303
q
Th1 cells
IFNγ+ CD4+ T cells in Brain (10³)
ns
r
Dᵇ Cre- Littermates
Cdh5-cre Dᵇ cKOs
CD11a+ CD8 T cells
ns
ns
0.0469
Meninges
Cervical LN
Brain
s
IV-
IV+
CD11a+ CD8 T cells in Brain
0.0482
ns
ns
ns
ns
t
% IFNγ+ of CD8+ T cells
ns
ns
ns
0.0158
0.0257
ns

Figure 6

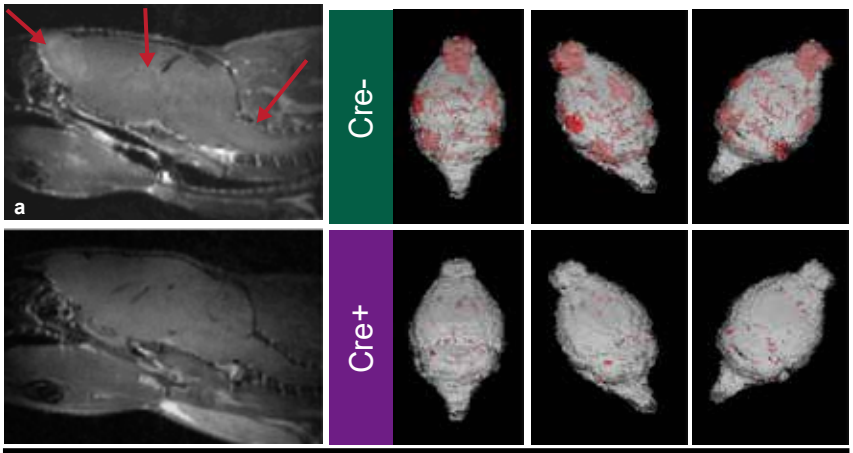
a
Cre-
Cre+

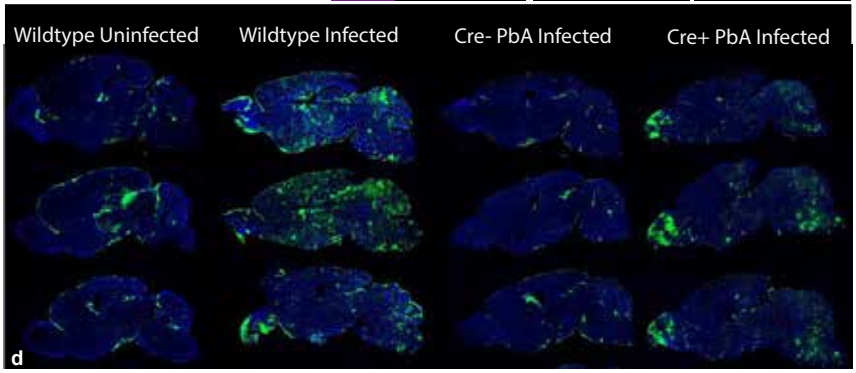
Wildtype Uninfected
Wildtype Infected
Cre- PbA Infected
Cre+ PbA Infected
d

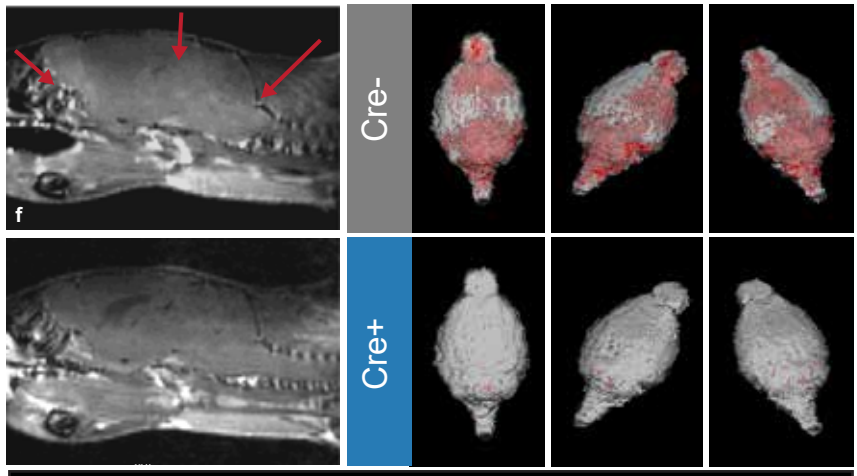
f
Cre-
Cre+

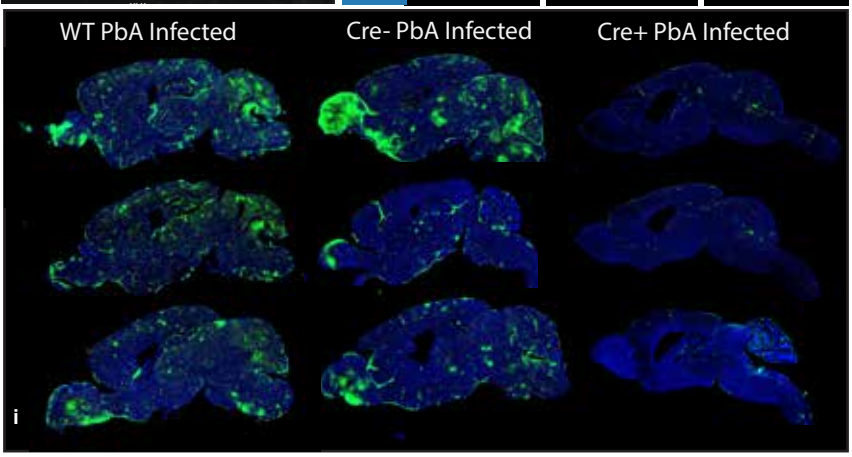
WT PbA Infected
Cre- PbA Infected
Cre+ PbA Infected
i

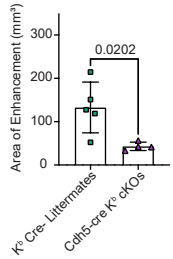
b
Area of Enhancement (mm³)
300
200
100
0
0.0202
Kᵇ Cre- Littermates
Cdh5-cre Kᵇ cKOs

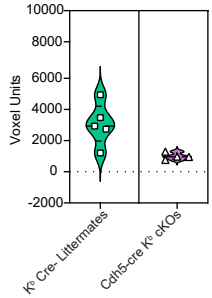
c
Voxel Units
10000
8000
6000
4000
2000
0
-2000
Kᵇ Cre- Littermates
Cdh5-cre Kᵇ cKOs

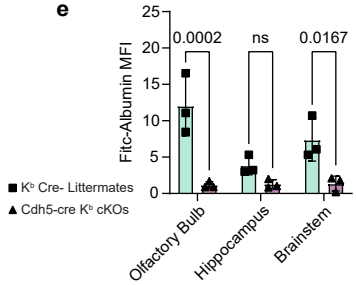
e
Fitc-Albumin MFI
25
20
15
10
5
0
0.0002
ns
0.0167
Kᵇ Cre- Littermates
Cdh5-cre Kᵇ cKOs
Olfactory Bulb
Hippocampus
Brainstem

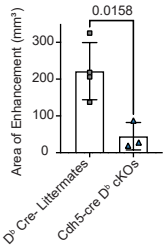
g
Area of Enhancement (mm³)
300
200
100
0
0.0158
Dᵇ Cre- Littermates
Cdh5-cre Dᵇ cKOs

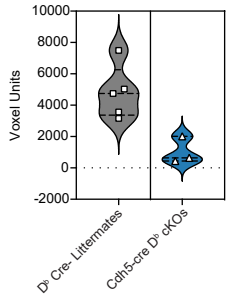
h
Voxel Units
10000
8000
6000
4000
2000
0
-2000
Dᵇ Cre- Littermates
Cdh5-cre Dᵇ cKOs

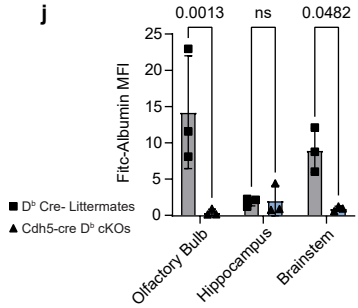
j
Fitc-Albumin MFI
25
20
15
10
5
0
0.0013
ns
0.0482
Dᵇ Cre- Littermates
Cdh5-cre Dᵇ cKOs
Olfactory Bulb
Hippocampus
Brainstem

Figure 7

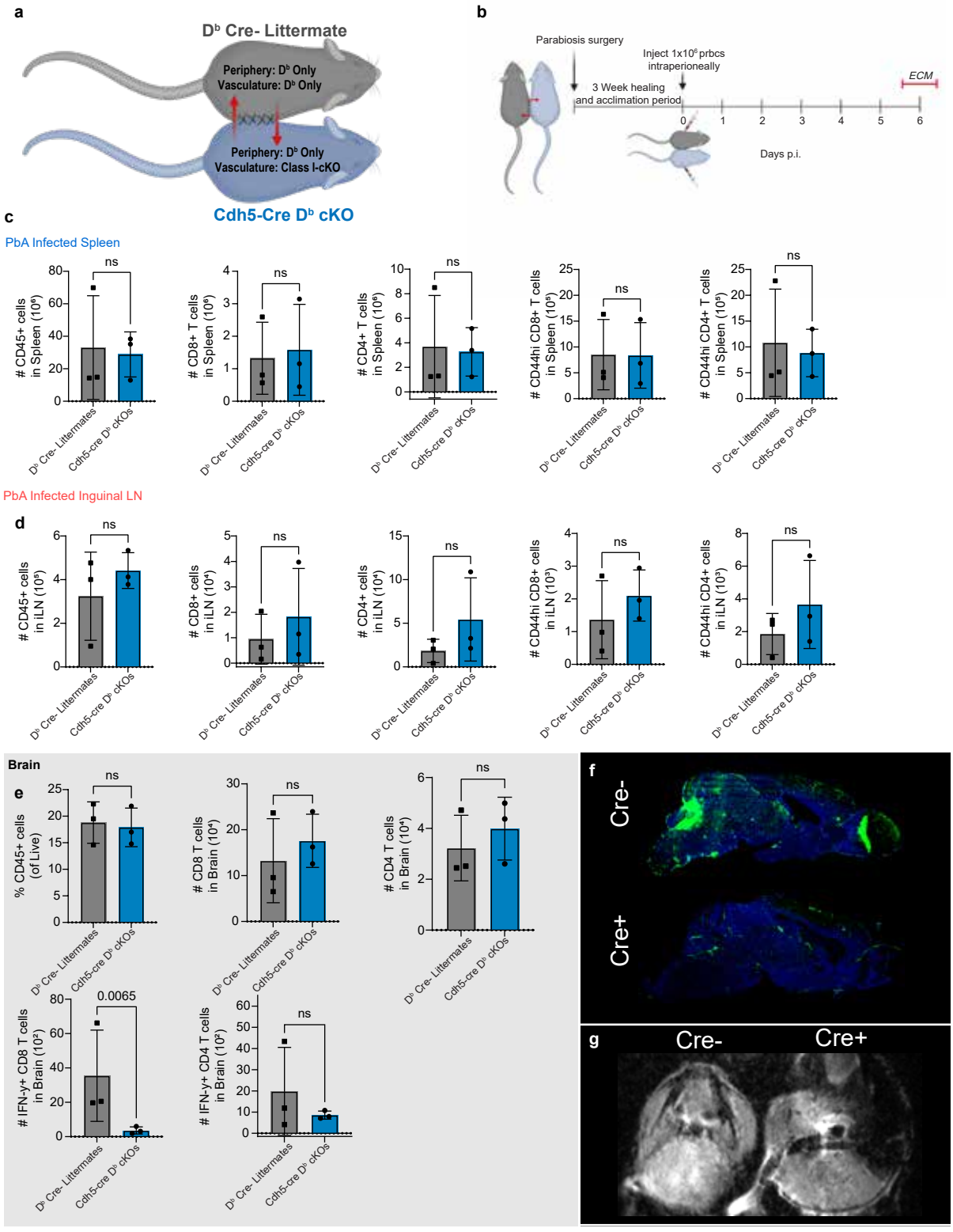
a
Dᵇ Cre- Littermate
Periphery: Dᵇ Only
Vasculature: Dᵇ Only
Periphery: Dᵇ Only
Vasculature: Class I-cKO
Cdh5-Cre Dᵇ cKO
b
Parabiosis surgery
Inject 1x10⁶ prbcs intraperioneally
3 Week healing and acclimation period
ECM
0 1 2 3 4 5 6
Days p.i.
c
PbA Infected Spleen
CD45+ cells in Spleen (10⁶)
CD8+ T cells in Spleen (10⁶)
CD4+ T cells in Spleen (10⁶)
CD44hi CD8+ T cells in Spleen (10⁵)
CD44hi CD4+ T cells in Spleen (10⁵)
ns
Dᵇ Cre- Littermates
Cdh5-cre Dᵇ cKOs
PbA Infected Inguinal LN
d
CD45+ cells in iLN (10⁵)
CD8+ cells in iLN (10⁴)
CD4+ cells in iLN (10⁴)
CD44hi CD8+ cells in iLN (10³)
CD44hi CD4+ cells in iLN (10³)
Brain
e
% CD45+ cells (of Live)
# CD8 T cells in Brain (10⁴)
# CD4 T cells in Brain (10⁴)
# IFN-γ+ CD8 T cells in Brain (10²)
# IFN-γ+ CD4 T cells in Brain (10²)
0.0065
f
Cre-
Cre+
g
Cre-
Cre+

Figure 8

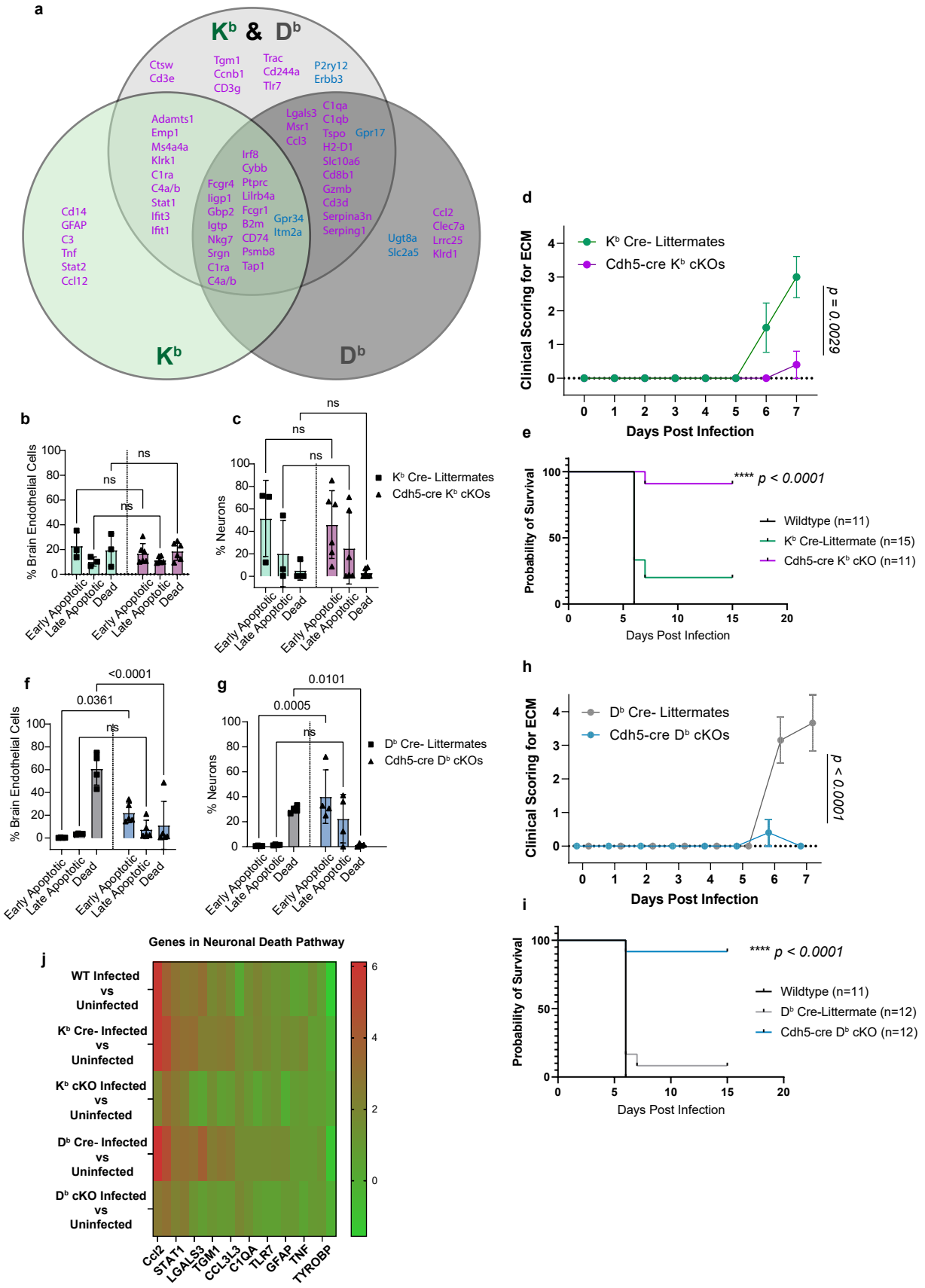
a
Kᵇ & Dᵇ
Ctsw
Cd3e
Tgm1
Ccnb1
CD3g
Trac
Cd244a
Tlr7
P2ry12
Erbb3
Adamts1
Emp1
Ms4a4a
Klrk1
C1ra
C4a/b
Stat1
Ifit3
Ifit1
Lgals3
Msr1
Ccl3
C1qa
C1qb
Tspo
Gpr17
H2-D1
Slc10a6
Cd8b1
Gzmb
Cd3d
Serpina3n
Serping1
Irf8
Cybb
Ptprc
Lilrb4a
Fcgr1
B2m
CD74
Psmb8
Tap1
Fcgr4
Iigp1
Gbp2
Igtp
Nkg7
Srgn
C1ra
C4a/b
Gpr34
Itm2a
Cd14
GFAP
C3
Tnf
Stat2
Ccl12
Ugt8a
Slc2a5
Ccl2
Clec7a
Lrrc25
Klrd1
Kᵇ
Dᵇ
b
% Brain Endothelial Cells
ns
Early Apoptotic
Late Apoptotic
Dead
c
% Neurons
Kᵇ Cre- Littermates
Cdh5-cre Kᵇ cKOs
d
Clinical Scoring for ECM
Kᵇ Cre- Littermates
Cdh5-cre Kᵇ cKOs
p = 0.0029
Days Post Infection
e
Probability of Survival
**** p < 0.0001
Wildtype (n=11)
Kᵇ Cre-Littermate (n=15)
Cdh5-cre Kᵇ cKO (n=11)
Days Post Infection
f
% Brain Endothelial Cells
<0.0001
0.0361
ns
g
% Neurons
0.0101
0.0005
ns
Dᵇ Cre- Littermates
Cdh5-cre Dᵇ cKOs
h
Clinical Scoring for ECM
Dᵇ Cre- Littermates
Cdh5-cre Dᵇ cKOs
p < 0.0001
Days Post Infection
i
Probability of Survival
**** p < 0.0001
Wildtype (n=11)
Dᵇ Cre-Littermate (n=12)
Cdh5-cre Dᵇ cKO (n=12)
Days Post Infection
j
Genes in Neuronal Death Pathway
WT Infected vs Uninfected
Kᵇ Cre- Infected vs Uninfected
Kᵇ cKO Infected vs Uninfected
Dᵇ Cre- Infected vs Uninfected
Dᵇ cKO Infected vs Uninfected
Ccl2
STAT1
LGALS3
TGM1
CCL3L3
C1QA
TLR7
GFAP
TNF
TYROBP

Supplementary Figure 1

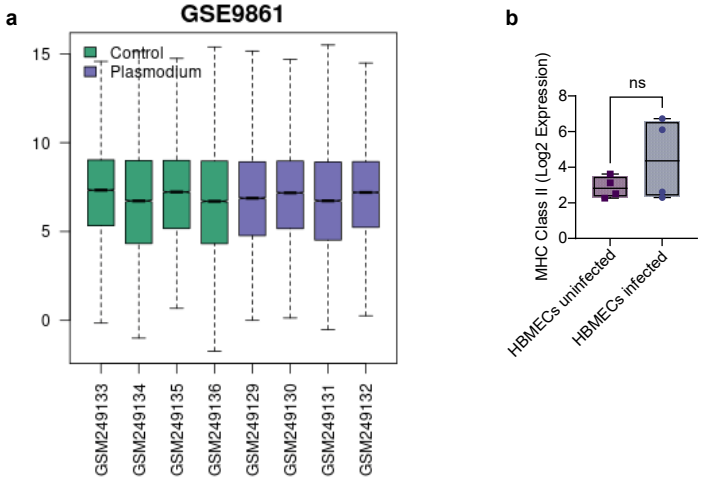

Supplementary Figure 2

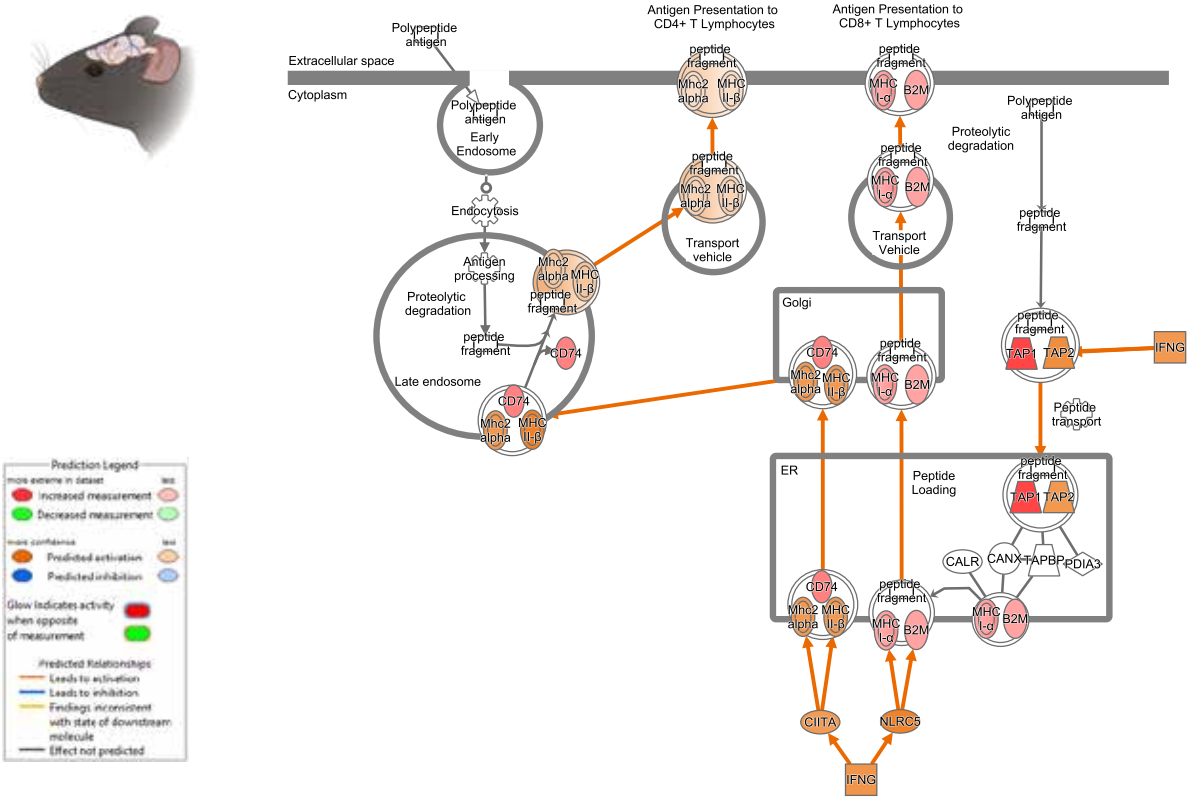

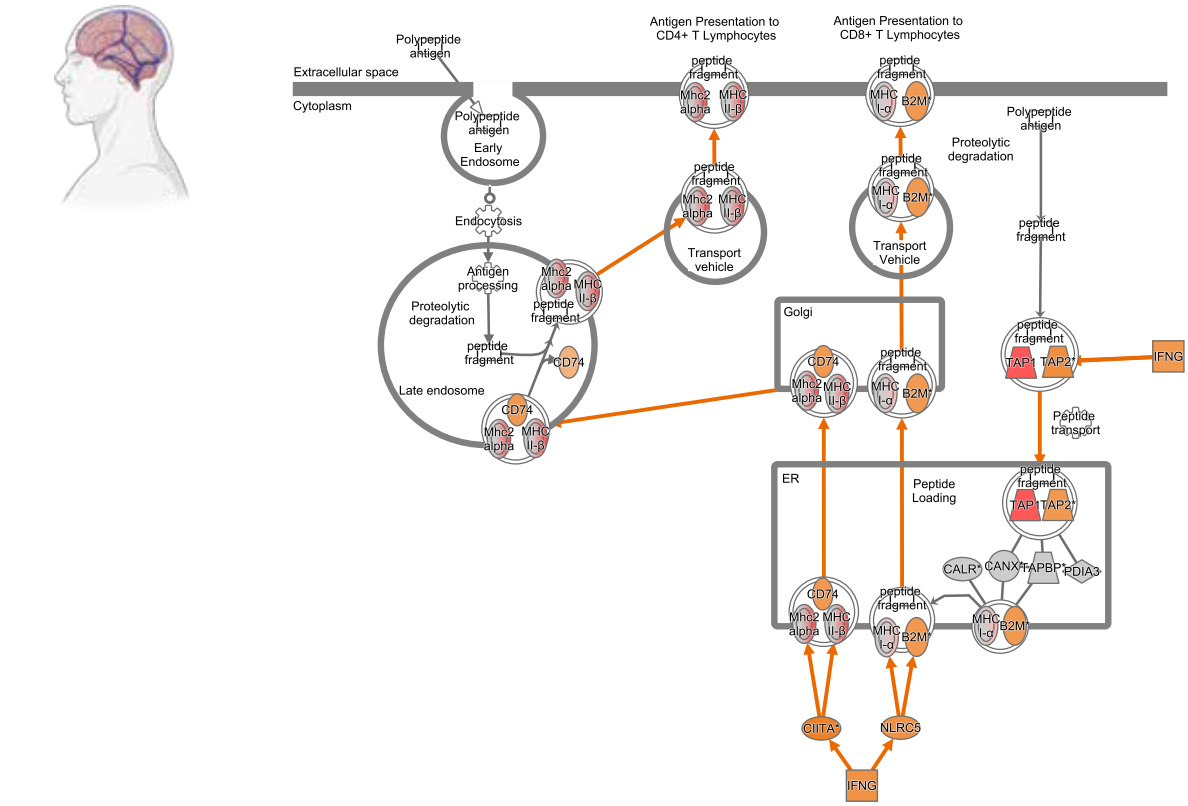

Supplementary Figure 3

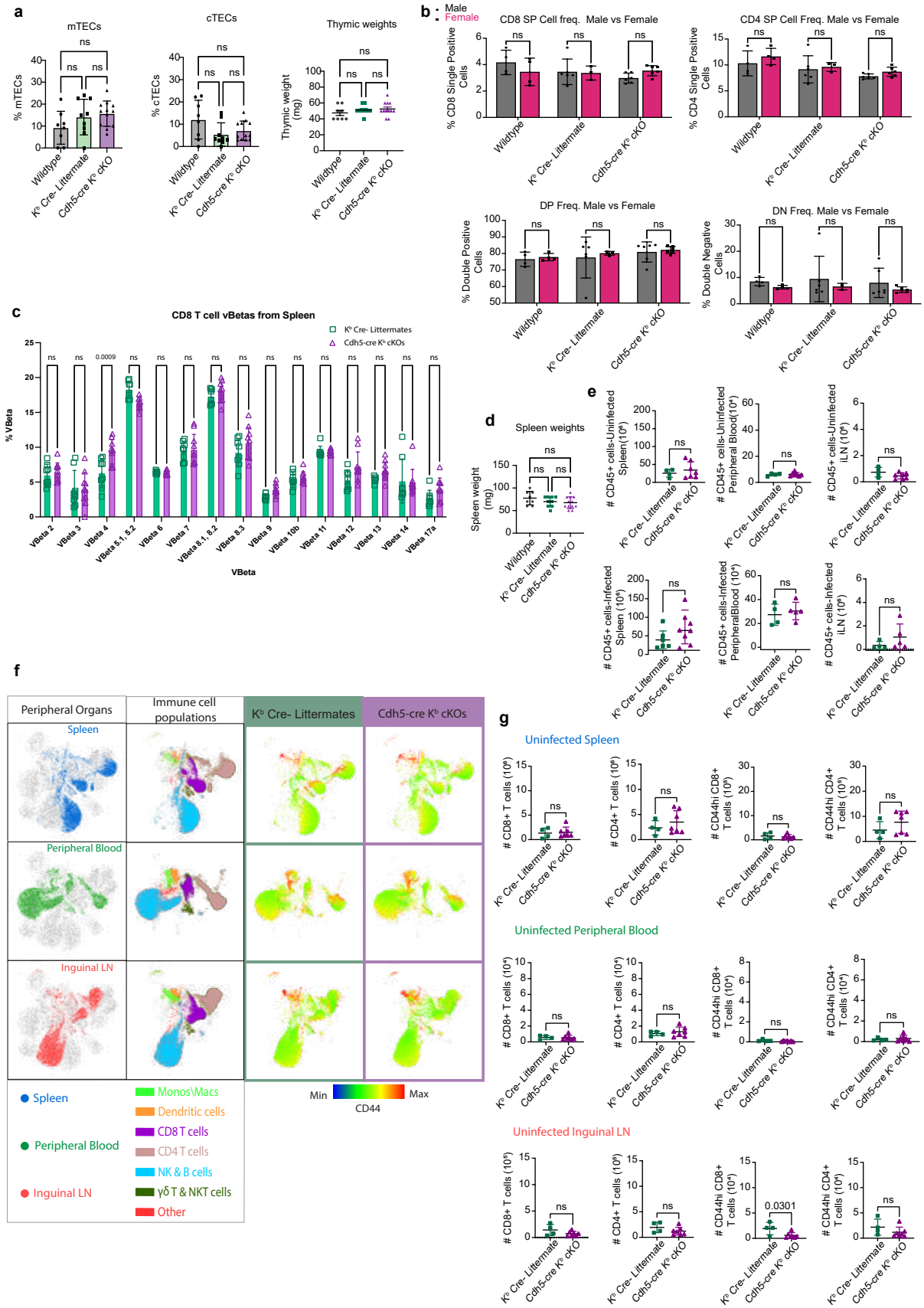

Supplementary Figure 4

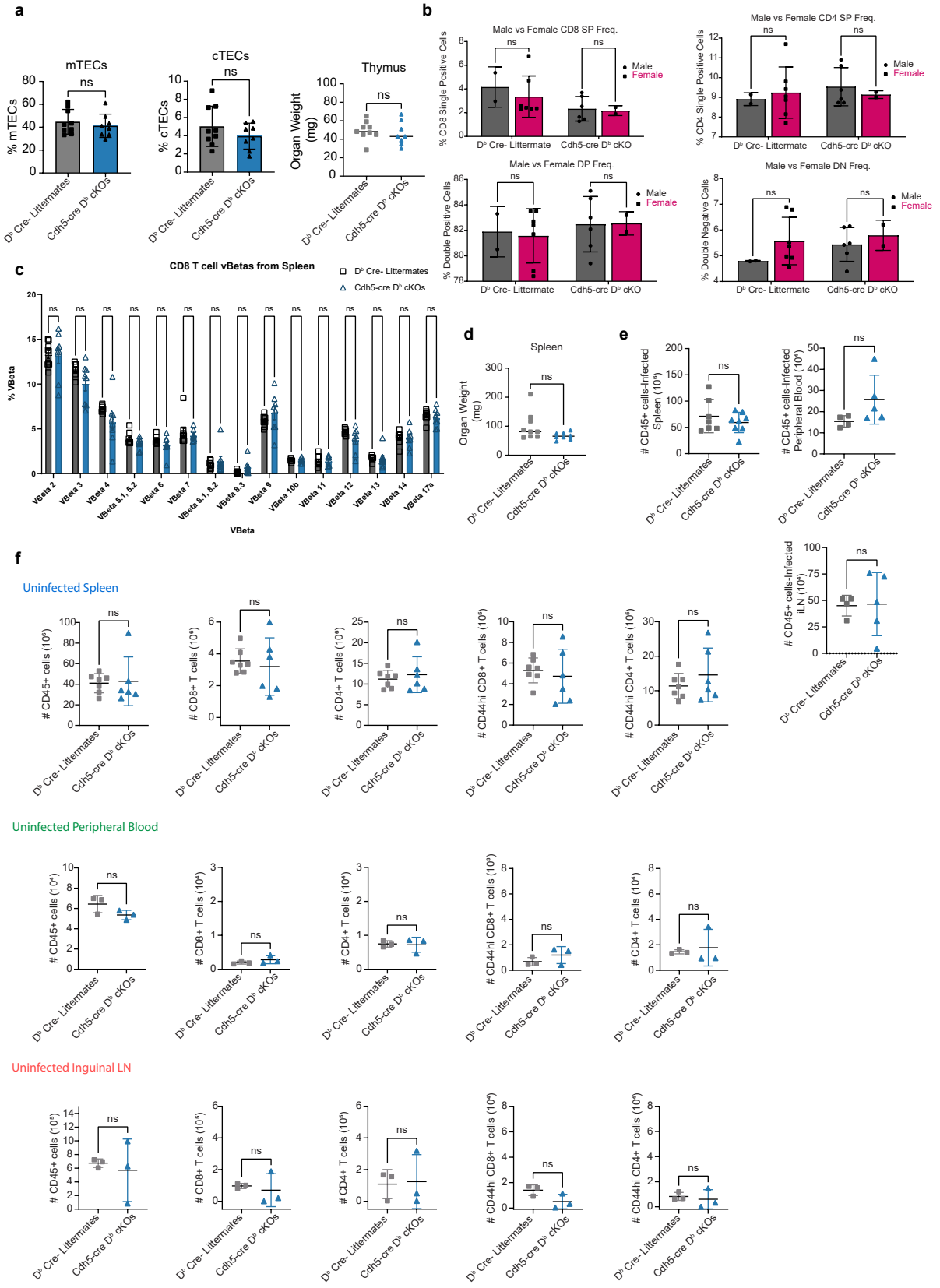

Supplementary Figure 5

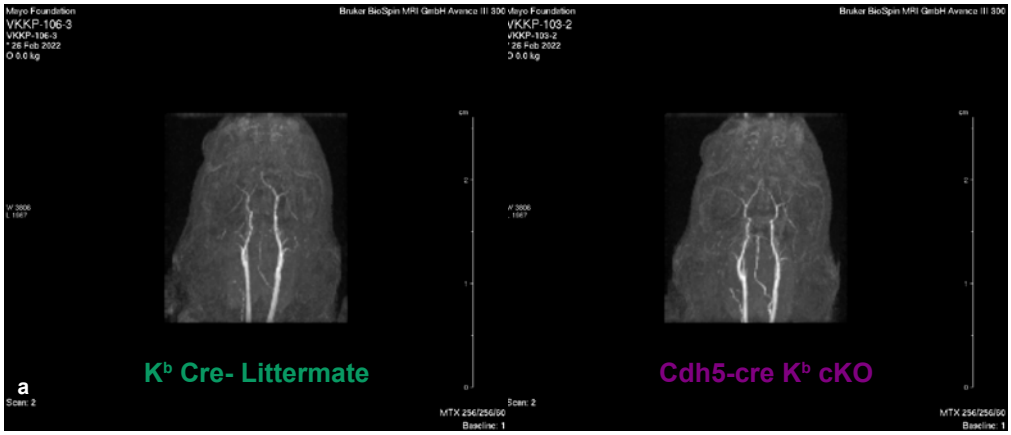

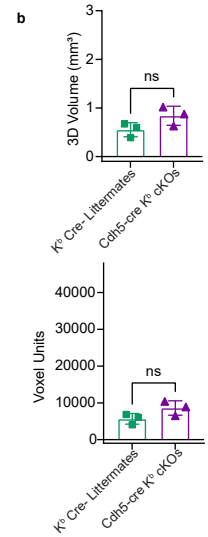

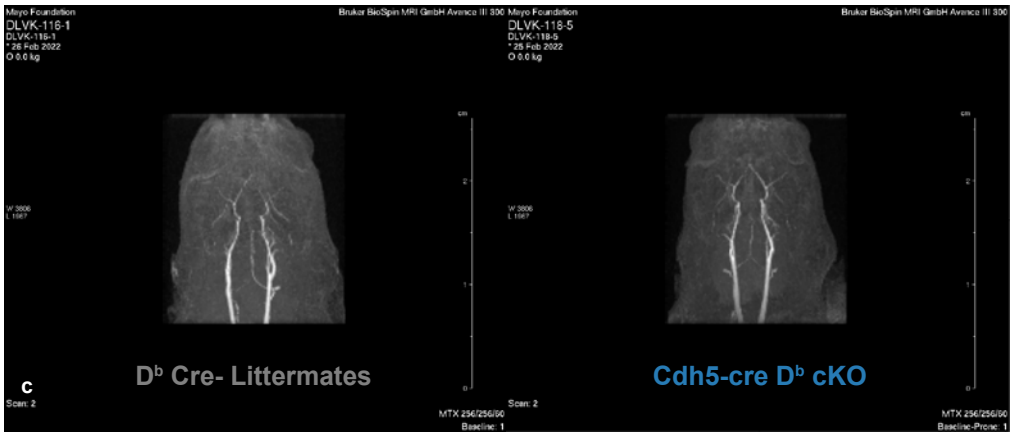

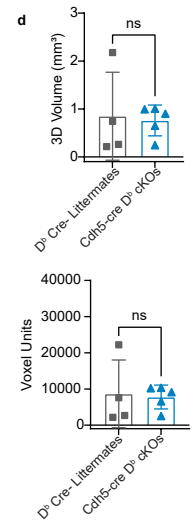

Supplementary Figure 6

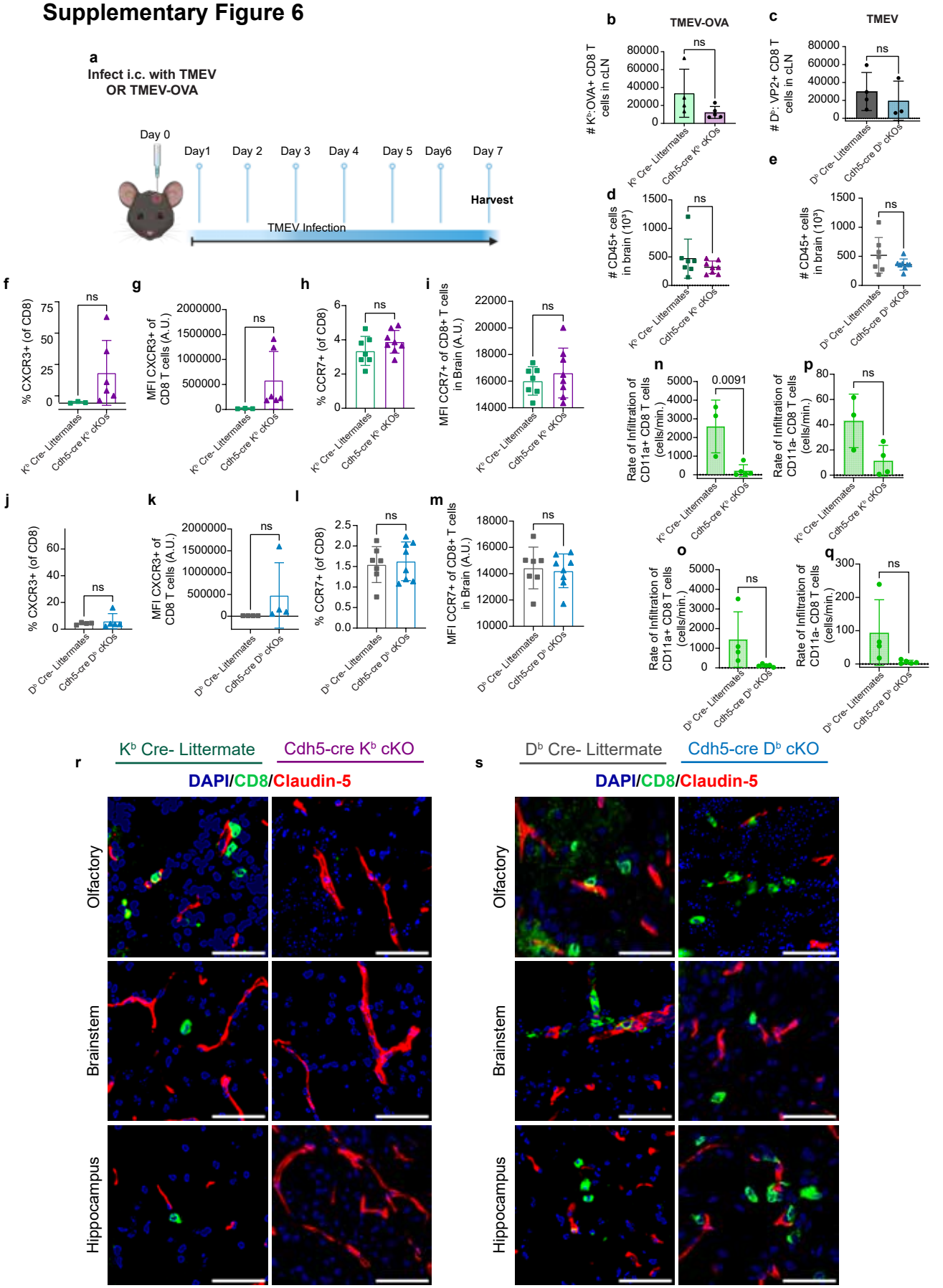

Supplementary Figure 7

a

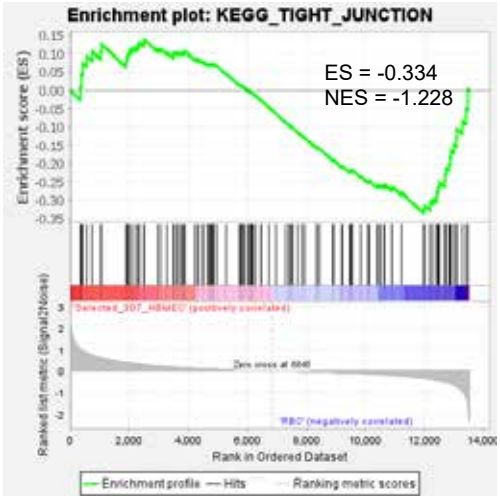

b

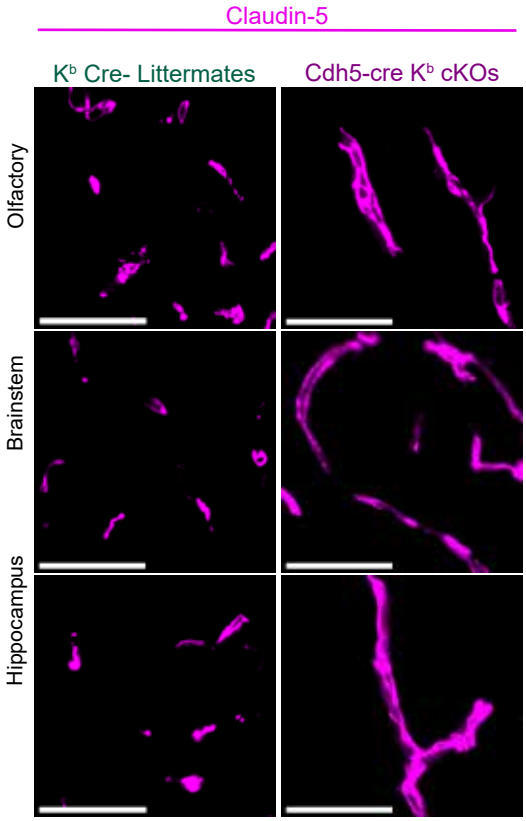

c

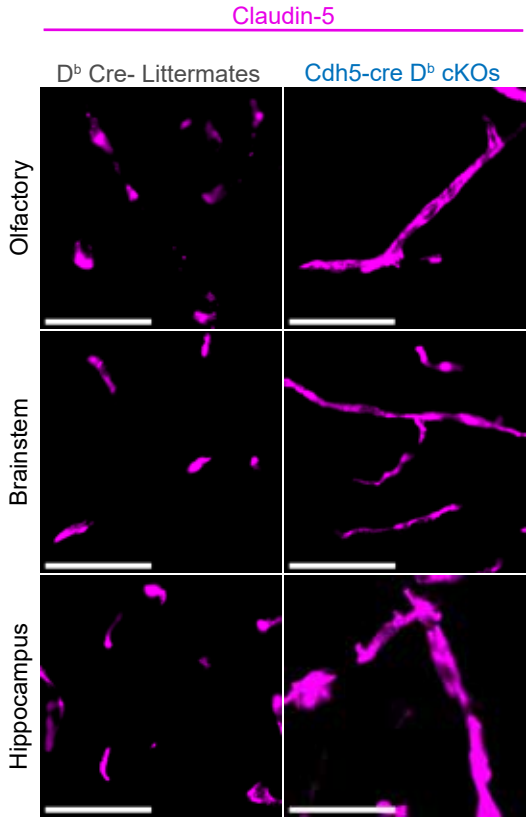
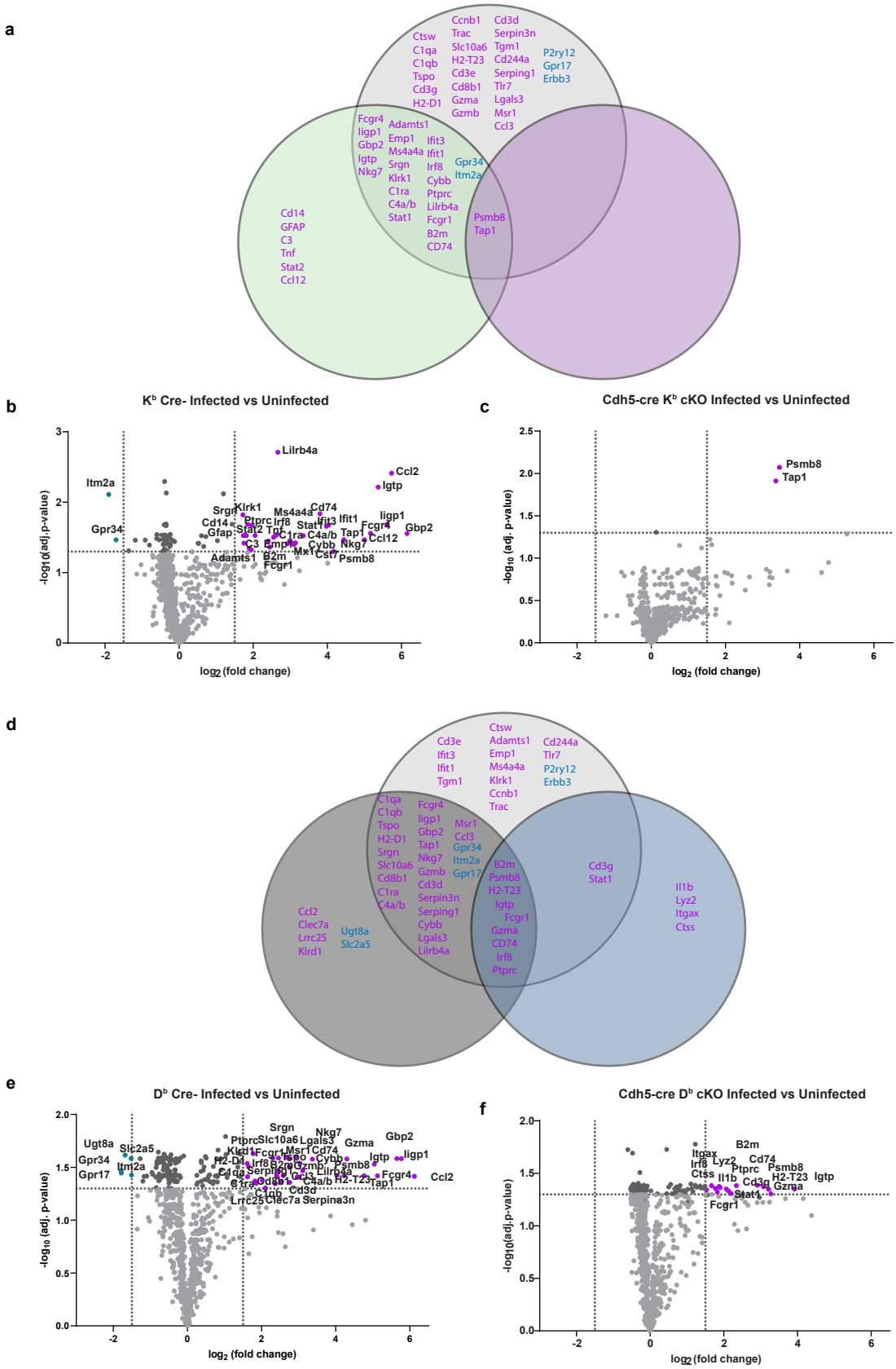
Supplementary Figure 8